

## 2. DATA REPORT: PETROLOGY AND GEOCHEMISTRY OF FRESH, RECENT DACITE LAVAS AT PUAL RIDGE, PAPUA NEW GUINEA, FROM AN ACTIVE, FELSIC- HOSTED SEAFLOOR HYDROTHERMAL SYSTEM<sup>1</sup>

D.J. Miller,<sup>2</sup> D.A. Vanko,<sup>3</sup> and H. Paulick<sup>4</sup>

### ABSTRACT

Leg 193 was the fourth Ocean Drilling Program expedition focusing on understanding subseafloor hydrothermal systems. This program was the first to combine studies of the volcanology, structure, hydrology, mineralization, and microbiology of a subseafloor hydrothermal system hosted by felsic rocks by coring at the PACMANUS hydrothermal field in the Manus Basin, Papua New Guinea. The study examines only the petrology and bulk rock and mineral chemistry of the freshest and most morphologically youthful lava flows recovered from the shallowest drill cores at the four sites occupied during Leg 193. There are subtle but distinct petrographic and geochemical variations between the closely spaced sites.

### INTRODUCTION

The Ocean Drilling Program (ODP) has, over the last 10 years, dedicated four expeditions to investigations into the subsurface nature of three different manifestations of seafloor hydrothermal systems. Studies of cores recovered from the hydrothermal mound in the Atlantic discovered during the Trans-Atlantic Geotraverse cruise (Humphris,

<sup>1</sup>Miller, D.J., Vanko, D.A., and Paulick, H., 2006. Data report: petrology and geochemistry of fresh, recent dacite lavas at Pual Ridge, Papua New Guinea, from an active, felsic-hosted seafloor hydrothermal system. *In* Barriga, F.J.A.S., Binns, R.A., Miller, D.J., and Herzig, P.M. (Eds.), *Proc. ODP, Sci. Results*, 193: College Station, TX (Ocean Drilling Program), 1–31. doi:10.2973/odp.proc.sr.193.208.2006  
<sup>2</sup>Integrated Ocean Drilling Program, Texas A&M University, 1000 Discovery Drive, College Station TX, 77845-9574, USA.  
[miller@iodp.tamu.edu](mailto:miller@iodp.tamu.edu)

<sup>3</sup>Department of Physics, Astronomy, and Geosciences, Towson University, 8000 York Road, Towson MD 21252-0001, USA.

<sup>4</sup>Mineralogisches und petrologisches Institut, Universität Bonn, Poppelsdorfer Schloss, 53115 Bonn, Germany.

Herzig, Miller, et al., 1996; Herzig, Humphris, Miller, and Zierenberg, 1998) explored the interaction between mid-ocean-ridge basalt (MORB) and hydrothermal fluid, while expeditions to Juan de Fuca Ridge (Davis, Mottl, Fisher, et al., 1992; Mottl, Davis, Fisher, and Slack, 1994; Fouquet, Zierenberg, Miller, et al., 1998; Zierenberg, Fouquet, Miller, and Normark, 2000) and to Escanaba Trough (Fouquet, Zierenberg, Miller, et al., 1998; Zierenberg, Fouquet, Miller, and Normark, 2000) examined hydrothermal processes in marine environments with high sedimentation rates. These expeditions demonstrated that the chemistry of seawater (Butterfield et al., 1994; Tivey et al., 1998; James et al., 1998) and the ocean crust (Kurnosov et al., 1994; Honnorez et al., 1998; Humphris et al., 1998; Stuart et al., 1999) are both intimately related to hydrothermal circulation. Additional interest in the ODP expeditions was fueled by the understanding that each of the systems investigated host mineral deposits that are analogous to ore deposits on land (Duckworth et al., 1994; Krasnov et al., 1994; Hannington et al., 1998; Zierenberg et al., 1998) and that they support unique seafloor and subseafloor biological communities (Reysenbach et al., 1998; Cragg et al., 2000; Summit et al., 2000). As a result of each of these expeditions, hypotheses relative to the formation and evolution of ancient ore deposits were either validated or revised (e.g., Duckworth et al., 1994; Humphris et al., 1995; Hannington et al., 1998; Herzig et al., 1998; Zierenberg et al., 1998).

The fourth expedition in this series was targeted at the PACMANUS (named after participants in the discovery team, Papua New Guinea, Australia, and Canada and the location of the expedition) hydrothermal system in the eastern Manus Basin (Fig. F1A) on top of Pual Ridge (Fig. F1B). This volcanic edifice is 1–1.5 km wide, 20 km long, and rises 500–600 m above the surrounding ocean floor (Fig. F1C). Previous dredge and submersible-based sampling demonstrated that it consists mainly of dacite and rhyodacite lava flows (Binns and Scott, 1993; Binns et al., 1996b; Waters and Binns, 1998). Trace element and isotopic analyses of the high-silica rhyodacite of Pual Ridge (Binns et al., 1996b; Woodhead and Johnson, 1993) suggest that the felsic lavas may have a geochemical affinity to the subareal volcanic rocks of New Britain. The descriptions of this area are the result of several expeditions including PACMANUS (Franklin 1991, 1993, 1996, and 1997), EDISON-I (Sonne, 1994), ManusFlux (Yokosuka, 1995), BIOACCESS (Natsushima, 1996, 1998), and KODOS'99 (Onmuri, 1999) cruises. The primary objective of ODP Leg 193 was to combine studies of the volcanology, structure, hydrology, mineralization, and microbiology to develop a comprehensive model for this hydrothermal system. This would allow us to compare PACMANUS, a felsic-hosted system, to MORB-hosted systems and ancient ore bodies.

Felsic volcanic sequences associated with convergent margins (island arcs) may host economic deposits of massive sulfides including base and precious metal mineralization. PACMANUS represents an environment where surface sampling revealed elevated concentrations of Au, Ag, and Pb (Herzig and Hannington, 2000). Our goal was to delve into the subsurface to determine the extent of and controls on mineralization in this environment.

Despite the extensive seafloor exposure of high-temperature sulfide chimneys and diffuse hydrothermal fluid reaction zones, subsurface mineralization was rare, indicating a very young mineralizing system (Shipboard Scientific Party, 2002a). However, in every hole that penetrated more than a few meters into the subsurface, pervasive hydrother-

F1. PACMANUS and drill sites, p. 13.



mal alteration indicates long-lived active hydrothermal circulation. Shipboard reconnaissance studies indicated that each sampled site had distinct mineralogical and geochemical characteristics suggesting the possibility of separate sources for lavas or at least distinct evolutionary trends.

## GEOLOGIC SETTING AND PREVIOUS WORK

The Manus backarc basin is set between opposed fossil (Manus Trench) and active (New Britain Trench) subduction zones. A chain of young arc volcanoes has formed above the north-dipping Wadati-Benioff Zone associated with the New Britain Trench, along the concave northern side of New Britain (Bismarck or New Britain arc) (Johnson, 1976). According to Taylor (1979), basement underlying the central Manus Basin may be predominantly basaltic crust formed in an earlier phase of backarc spreading that commenced ~5 m.y. ago. A series of neovolcanic edifices extends en echelon across the Eastern Manus Basin, wherein seismic data are consistent with rifting over the last ~1 m.y.

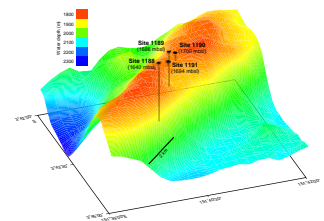
The PACMANUS hydrothermal field targeted by Leg 193 is located on the crest of Pual Ridge, a prominent felsic neovolcanic edifice with negligible sediment cover. Mapping by submersible and camera tows indicates the ridge is built of stacked, subhorizontal 5- to 30-m-thick lava flows (Waters et al., 1996).

Isolated hydrothermal deposits were photographed along 13 km of the main crest of Pual Ridge (Binns and Scott, 1993; Binns et al., 1995, 1996a, 1997a, 1997b). The most active hydrothermal areas occur in the center of this zone between two low knolls on the ridge crest. Extensive bottom-tow photography and manned submersible observation identified four principal areas of hydrothermal activity, including sulfide chimneys and areas of diffuse venting.

ODP sites occupied four targets on Pual Ridge (Fig. F2). Site 1188 (Snowcap) is an area of diffuse venting where the deepest penetration (~400 m) into the ridge was achieved. Roman Ruins (Site 1189) is characterized by closely packed simple and complex columnar chimneys as high as 20 m. Site 1190 is a reference site in an area devoid of visible hydrothermal activity. Satanic Mills (Site 1191) is an area of active black smoker chimneys.

At Snowcap (Site 1188), there is a 35-m-thick layer of fresh, moderate porphyritic dacite (sampled in Hole 1188A) overlying intensely altered aphyric dacite. This lava flow occupies a local knoll on the crest of Pual Ridge reaching 1640 meters below sea level (mbsl). At Roman Ruins, fresh aphyric dacite is restricted to <10 meters below seafloor (mbsf) in Hole 1189A, which was drilled beside a chimney on the edge of the hydrothermal discharge area. Hole 1189B is at the base of an active black smoker chimney and was cased to a depth of 30 mbsf. Below a sequence of strongly altered dacite, including a hydrothermal stockwork zone, there are less altered dacite lavas and breccia units at >120 mbsf. Here, a thick, vesicular, coherent dacite was recovered and petrographic (abundant, subvertically aligned vesicles) (Shipboard Scientific Party, 2002c) and geophysical evidence (steeply inclined top and base contacts apparent in electrical resistivity images) (Bartetzko et al., 2003) indicate a dikelike discordant geometry of this body. A sample of this fresh dacite is included in Table T1 (Sample 193-1189B-11R-3, 3 cm; 129.72 mbsf).

F2. Pual Ridge, p. 15.



T1. Bulk rock geochemistry, p. 26.

The ODP sites to the northwest of Snowcap (Satanic Mills and the reference site) are located at 1680–1690 mbsl (Fig. F2), and the holes penetrated aphyric or sparsely porphyritic dacite. Fresh samples of these dacite types were recovered at Sites 1190 and 1191, where holes reached <20 mbsf.

## METHODOLOGY

A total of 32 polished thin sections were prepared from samples of fresh dacite. In addition, 31 samples of fresh to incipiently altered dacite from the shipboard thin section collection were included in our petrographic analyses. Minerals and glass were analyzed for major element oxide and minor (>0.2%) and trace elements (Table T2). Mineral chemistry on samples from Sites 1188, 1190, and 1191 was determined by electron microprobe at the Texas A&M Department of Geology and Geophysics (College Station, Texas) with the Cameca SX-50 Superprobe using a combination of glass, mineral, and pure metal standards. Phases were analyzed using an accelerating voltage of 15 keV and count times from 20 to 30 s with a 1- to 10- $\mu$ m-wide beam. Mineral chemistry on samples from Site 1188 was determined by the JEOL JXA-8600 Superprobe in the Geology Department at the University of Georgia, using 15-keV accelerating voltage, 5- to 10- $\mu$ m beam, and well-characterized natural and synthetic mineral standards.

The concentrations of major and trace elements of 28 fresh bulk rock samples were determined. Samples marked “JM” in Table T1 were analyzed by LiBO<sub>2</sub> fusion followed by inductively coupled plasma (ICP) spectrometry. Major element oxides were determined by ICP–atomic emission spectrometry and trace elements by ICP–mass spectrometry (MS). These analyses were performed by Acme Analytical Laboratories, Vancouver, British Columbia, Canada. Replicate samples and U.S. Geological Survey standard reference materials were included in the analytical suite as unknowns to ensure accuracy and precision. Samples marked “HP” in Table T1 were analyzed by X-ray fluorescence for major elements and selected trace elements (Ba, Rb, Sr, Y, and Zr). All other trace elements, including rare earth elements (REE) were analyzed by ICP-MS. Solutions were prepared using hydrofluoric and nitric acids under atmospheric conditions. A pair of interlaboratory standards compiled from ground wash core material was submitted during all of these analyses to ensure interlaboratory comparability. Data from these reference material analyses are included in Miller et al. (this volume).

## RESULTS

### Petrology

In general, the fresh dacites from PACMANUS are vesicular and glassy with variable amounts of feldspar microlites. The phenocryst assemblage includes plagioclase, pyroxene, and Ti-magnetite. Based on point counting of 23 thin sections (500–800 points each; data documented in Binns, Barriga, Miller, et al., 2002), three types of dacite can be distinguished: moderately porphyritic dacite (2%–3% plagioclase, 1% pyroxene, 0.5% Ti-magnetite), sparsely porphyritic dacite (0.5%–2% plagioclase, 0.1%–1% pyroxene; <0.1%–0.5% Ti-magnetite), and aphyric dacite ( $\leq$ 0.5% phenocrysts). Although determined attempt was made

---

T2. Mineral and glass compositions, p. 30.

---

to evaluate each piece of fresh volcanic rubble for indications of stratigraphic relevance (number of flows or cooling units), no such correlation was deemed possible. From Sites 1188, 1189, and 1190, only a few pieces of relatively fresh material were recovered (<50 smaller than fist-sized pieces in total) so only subtle inferences regarding recent volcanic stratigraphy are possible. More fresh dacite pieces (68) were recovered from Site 1191. However, even in pieces long enough to be considered oriented (25% of pieces recovered, of which only half were convincingly long enough to have escaped rotation in the core barrel) closely adjacent pieces show radically different orientations in vesicle flattening and alignment, suggesting most if not all recovered material was from disaggregated lava lobes.

## Site 1188 (Snowcap)

### *Megascopic Features*

The uppermost section sampled at Site 1188 (Cores 193-1188A-2R through -4R; Core 1R had no recovery) consists of 15 curated pieces of volcanic rock fragments. Fewer than half of the fragments are more than a few centimeters in longest dimension. The core is moderately vesicular plagioclase- and clinopyroxene-phyric dacite. In pieces long enough to suggest they are oriented, vesicles commonly show elongation (cigar-shaped in three dimensions rather than merely flattened) with a typically normal orientation with respect to the long axis of core, indicating horizontal flow on the seafloor; therefore, an intact lava flow was likely sampled. In the top of Core 193-1188A-7R, beneath an interval of aphyric, pervasively altered dacite, three pieces of fresh dacite were recovered. In all megascopic and microscopic features, these pieces appear identical to the fragments in Cores 193-1188A-2R through 4R, and we can find no reason to contend the interpretation of shipboard scientists (Shipboard Scientific Party, 2002b) that these were pieces of rubble from the upper part of the section that fell into the hole and were resampled during the coring operation. Therefore, even with the low recovery, we concur with the shipboard interpretation that the unaltered, morphologically youthful part of the lava section at this site is no more than ~35 m thick.

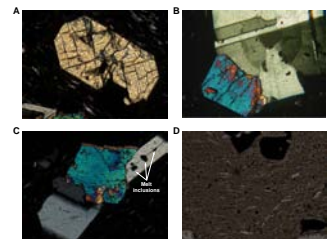
### *Phenocrysts*

Plagioclase and pyroxene (predominantly clinopyroxene with minor orthopyroxene) are euhedral to subhedral (Fig. F3A) and <2 mm long, with rare exceptions. Twinned feldspar grains are common (Fig. F3B), but oscillatory zoning is less common. Only rare evident quench textures or skeletal growth features suggest little radical undercooling of the lava. Melt inclusions are common in plagioclase (Fig. F3C) and more rare in pyroxene. Pyroxene forms elongate prisms (Fig. F3A), commonly broken but with euhedral faces. Small subhedral magnetite phenocrysts are rare (Fig. F3D) and commonly occur proximal to plagioclase phenocrysts. Magnetite microphenocrysts <0.2 mm in length are common as inclusions in plagioclase and pyroxene.

### *Groundmass*

Groundmass in virtually all thin sections examined is 55%–65% fresh, brown, volcanic glass. The groundmass glass is permeated with 35%–45% acicular plagioclase microlites with generally a 10:1 aspect ratio. Very fine grained pyroxene and opaque minerals are also present. In

F3. Phenocrysts, p. 16.



most thin sections, the groundmass microlites are strongly flow aligned (Fig. F3).

#### *Vesicles*

Vesicularity appears to decrease downhole from 10% in Core 193-1188A-2R to 5% in Core 4R. The majority of the vesicles are flattened and flow aligned parallel to microlite fabric in the groundmass.

### **Site 1189 (Roman Ruins)**

#### *Megascopic Features*

Only the uppermost four pieces of core fragment from Site 1189 are fresh volcanic rocks. These are vesicular but virtually aphyric. The rest of Core 193-1189A-1R and the upper four pieces of Core 2R are moderately altered but are aphyric to very sparsely plagioclase phyric dacite.

#### *Phenocrysts*

Very rare, rounded microphenocrysts of feldspar occur in the moderately altered samples from Cores 193-1189A-1R and 2R and in similarly altered samples from deeper in the hole (Fig. F4A). Considering the rounded plagioclase morphology and the observation that some feldspars exhibit normal zoning and some show reverse zoning suggests that plagioclase was on the liquidus during emplacement of the dacite at Roman Ruins.

#### *Groundmass and Vesicles*

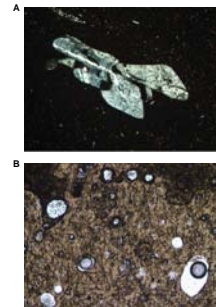
Fresh, brown glass constitutes the groundmass of the upper few pieces of core from Site 1189. In the freshest samples, 15%–25% plagioclase microlites show no preferred orientation despite the flattened and aligned vesicles (30% by volume of the rock). In one of the least altered samples from Core 193-1189A-2R, vesicles are rounded and plagioclase microlites have a distinct jackstraw distribution (Fig. F4B). The much more extensive vesiculation in the upper part of Core 193-1189A-1R, the distinct change in alteration character and vesicle morphology, and the change from complete absence to rare occurrence of detectable phenocrysts suggest that the lavas below Core 193-1189A-1R could be a separate flow unit.

### **Site 1190 (Reference Site)**

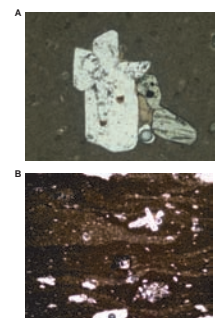
#### *Megascopic Features*

Samples of fresh volcanic rock from the reference site are moderately vesicular and sparsely plagioclase and pyroxene phyric (Fig. F5A). Three holes were drilled, with no recovery from the first, only one cored interval from the second, and a total of just over 13 m penetration at the third with <25 fragments of volcanic rock recovered. None of these pieces were large enough to be considered oriented with respect to the way up. The samples are all sparsely plagioclase phyric, and we can detect no features to depart from the shipboard interpretation that all the pieces of rock recovered are from a single flow. Because the pieces have no distinguishing characteristics and none of the pieces are oriented, we have no criteria from which to infer whether or not the pieces are from a single flow or are part of pile of volcanic rubble.

F4. Microlites, p. 17.



F5. Rounded phenocrysts, p. 18.



### *Phenocrysts*

Plagioclase (virtually ubiquitously 2% by volume) is generally euhedral to subhedral and rarely exhibits zoning, but inclusions of magnetite and melt are common. Subtle rounding of phenocryst margins is common. Pyroxene is much less abundant than plagioclase and occurs as subhedral prisms with rounded corners and crystal edges. Magnetite phenocrysts are smaller than plagioclase or pyroxene but distinctly larger than groundmass phases. Glomerocrysts of plagioclase, pyroxene, and magnetite are common, and the groundmass glass surrounding these clusters of crystals is free of microlites (Fig. F5A). A discussion of this phenomenon can be found in the Site 1190 chapter of the Leg 193 *Initial Reports* volume (Shipboard Scientific Party, 2002d).

### *Groundmass and Vesicles*

Groundmass glass contains abundant acicular plagioclase microlites with fewer opaque grains and distinct flow banding manifested as dark and lighter wisps (Fig. F5B). The darker bands are more voluminous and have gradational to sharp boundaries with the lighter bands. The dark bands contain abundant microvesicles. The lighter bands have more abundant volcanic glass. This agrees with shipboard observations (Shipboard Scientific Party, 2002d), although shipboard samples were described with more abundant plagioclase microlites in the darker bands as well. The bands were interpreted to suggest that phase separation may have been favored where microlites were more abundant. However, even in flow banded areas, radial clusters of microlites are common, with some microlite alignment present. We also observe that the most striking difference between the bands is the proportion of glass to microvesicles and not a marked difference in plagioclase microlite abundance. Vesicle abundance ranges from 5% to 20%, and whereas most samples are characterized by flattened and elongated vesicles, a few (i.e., Sample 193-1190C-2R-1, 10–12 cm) have a distinctly bimodal vesicle distribution with small (0.2 mm) spherical and larger, >1 mm, flattened and aligned vesicles.

## **Site 1191 (Satanic Mills)**

### *Megascopic Features*

Fresh vesicular aphyric to sparsely plagioclase phyric dacite was recovered from the subsurface of the Satanic Mills hydrothermal site. Drilling penetrated ~20 mbsf. The most striking feature of the samples recovered from this location is the transition from fresh to incipiently altered to moderately altered rhyodacite within a few centimeters of the seafloor. The intensity of alteration at this site is lower relative to the pervasive alteration reported from deeper intervals at Sites 1188 and 1189 (Shipboard Scientific Party, 2002b, 2002c). Although a few pieces of fresh volcanic rock appear in deeper cores, because there is no morphologic or petrologic criteria to distinguish these as more recent flows, we interpret these as pieces of fresh material falling into the borehole during coring.

### *Phenocrysts*

Many thin sections are aphyric; however, subhedral to euhedral plagioclase is the most common phenocryst phase but rarely exceeds 1 mm in long dimension (Fig. F6). Rare pyroxene phenocrysts are less elongate, although they still appear slightly rounded. Magnetite phenocrysts are rare.

F6. Euhedral phenocrysts, p. 19.



### Groundmass and Vesicles

The groundmass from all fresh samples examined from Site 1191 comprise brown volcanic glass and fine, disseminated plagioclase microlites. The microlites commonly exhibit flow alignment. Vesicles are fairly abundant, exceeding 30% by volume in some samples. Several pieces have a distinctly bimodal vesicle distribution, with one set of small (average = 0.2 mm) spherical vesicles and another set of larger (>1 mm) flattened and aligned vesicles. With depth, there seems to be a decrease in the abundance of flattened and aligned vesicles, but the bimodal size distribution remains.

## Bulk Rock Chemistry

Data from nearly all samples plot near the dacite/rhyolite boundary in a total alkali vs. silica diagram (Fig. F7), and compositions (Table T1) are consistent with the field of bulk rock analyses for dredge samples from Pual Ridge compiled by Yang and Scott (2002). The data indicate lavas from Roman Ruins (Site 1189) are the most mafic (e.g., 64 wt% SiO<sub>2</sub>), whereas samples from the other sites were all more silica rich.

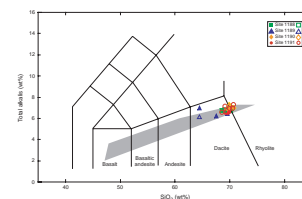
The uppermost lavas from Site 1189 have MgO of 1.8 wt% and elevated CaO relative to fresh lavas from other sites (Fig. F8). One of the rare, relatively fresh dacites sampled from ~130 mbsf at Site 1189 has an elevated MgO (1.3 wt%) as compared to the other sites sampled (0.7–0.9 wt%) but most closely resembles lavas from Sites 1188 and 1190 in terms of most major element oxides. Covariation diagrams of SiO<sub>2</sub> relative to other major element oxides (MgO, Al<sub>2</sub>O<sub>3</sub>, Fe<sub>2</sub>O<sub>3</sub>, CaO, and alkalis) exhibit consistent fractionation trends from the most primitive samples (Site 1189) to the most evolved (Site 1190).

Plots of TiO<sub>2</sub> vs. Zr and SiO<sub>2</sub> vs. Ti/Zr (Fig. F9) also illustrate the geochemical variability present in the fresh lavas from Pual Ridge, indicative of magmatic differentiation. Ba increases from 250 to >400 ppm, consistent with magmatic differentiation, although relatively high Ba (>500 ppm) may be indicative of incipient alteration. Chondrite-normalized REE compositions from all sites (N = 28) are indistinguishable, indicating derivation from a common parent (Fig. F10). The REE patterns of fresh dacites from the subsurface at PACMANUS show negative Eu anomalies with Eu/Eu\* values ranging from 0.98 to 0.69. A slight negative correlation between Eu/Eu\* and SiO<sub>2</sub> defined by most samples (Fig. F11) indicates the development of the Eu anomaly was probably associated with igneous fractionation processes. A weak positive correlation between Eu/Eu\* and CaO and a more well-developed positive correlation between Eu/Eu\* and Sr (Fig. F11) indicates plagioclase fractionation was an important process during the petrogenetic evolution of the dacitic magmas from Pual Ridge. A summary of key petrologic and geochemical data is in Table T3.

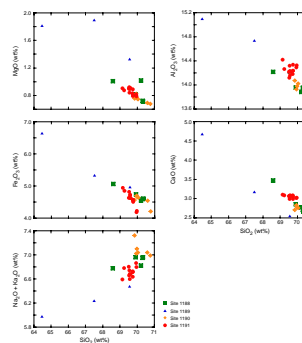
## Mineral Chemistry

Plagioclase compositions from fresh Site 1188 (Snowcap) lavas range from An<sub>37</sub> to An<sub>44</sub>. Clinopyroxene is Wo<sub>40</sub>-En<sub>40</sub>-Fs<sub>20</sub>, and orthopyroxene is Wo<sub>3.5</sub>-En<sub>55</sub>-Fs<sub>41.5</sub> (Table T3; Fig. F12). At Roman Ruins (Site 1189) the rare plagioclase phenocrysts are the most calcic plagioclase compositions analyzed from the Leg 193 fresh lava sample set, ranging from An<sub>49</sub> to An<sub>52</sub>. Plagioclase analyses from altered samples recovered from deeper at Site 1189 range from An<sub>40</sub> to An<sub>50</sub>. Plagioclase compositions

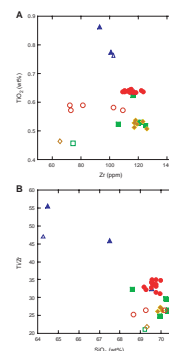
F7. Bulk rock compositions, p. 20.



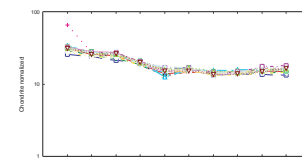
F8. SiO<sub>2</sub> covariation, p. 21.



F9. TiO<sub>2</sub> vs. Zr, p. 22.



F10. Chondrite-normalized REEs, p. 23.

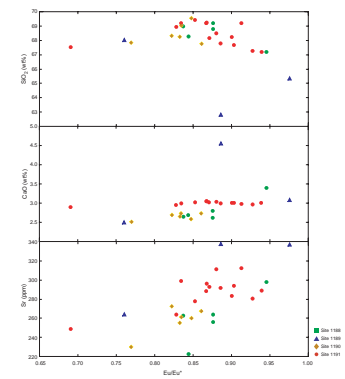


from Site 1190 (reference site) lavas are  $An_{43}$  to  $An_{47}$ , somewhat less calcic than the nearby Site 1189 lava but significantly more calcic than plagioclase sampled from Snowcap or Satanic Mills. Fresh lava from Site 1190 has orthopyroxene with the same composition as the Snowcap site, but clinopyroxene is slightly more calcic ( $Wo_{43}$ - $En_{38}$ - $Fs_{19}$ ). The Satanic Mills (Site 1191) plagioclase phenocrysts contain the lowest anorthite content ( $An_{35}$  to  $An_{40}$ ) measured in fresh lavas sampled during Leg 193. Clinopyroxene compositions appear identical to those from nearby Snowcap, but orthopyroxene ( $Wo_{3.7}$ - $En_{62}$ - $Fs_{34.3}$ ) contains lower iron and higher magnesium than samples from other locations.

## ACKNOWLEDGMENTS

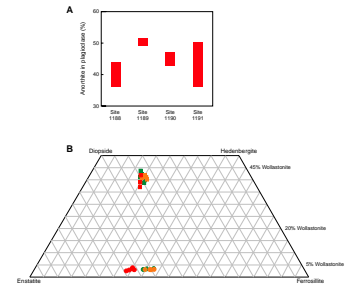
The authors acknowledge Sang-Mook Lee, who provided the bathymetry data from Lee (2000), and Katerina Petronotis, who processed the data to generate Figure F2. We also want to acknowledge reviews from Graziella Caprarelli, Vadim Kamenetsky, and Ray Binns. This research used samples and/or data provided by the Ocean Drilling Program (ODP). ODP is sponsored by the U.S. National Science Foundation (NSF) and participating countries under management of Joint Oceanographic Institutions (JOI), Inc. Funding for this research was provided by grants from U.S. Science Advisory Committee to D.J.M. and D.A.V. and from the German Research Foundation (DFG) to H.P.

**F11.** Eu/Eu\* covariation, p. 24.



**T3.** Data summary, p. 31.

**F12.** Anorthite content, p. 25.



## REFERENCES

- Andersen, D.J., Lindsley, D.H., and Davidson, P.M., 1993. QUILF: a Pascal program to assess equilibrium among Fe-Mg-Ti-oxides, pyroxenes, olivines, and quartz. *Comp. Geosci.*, 19:1333–1350. doi:10.1016/0098-3004(93)90033-2
- Bartetzko, A., Paulick, H., Iturrino, G., and Arnold, J., 2003. Facies reconstruction of a hydrothermally altered dacite extrusive sequence: evidence from geophysical downhole logging data (ODP Leg 193). *Geochem., Geophys., Geosyst.*, 4:1087. doi:10.1029/2003GC000575
- Binns, R.A., Barriga, F.J.A.S., Miller, D.J., et al., 2002. *Proc. ODP, Init. Repts.*, 193: College Station, TX (Ocean Drilling Program). doi:10.2973/odp.proc.ir.193.2002
- Binns, R.A., Parr, J.M., Scott, S.D., Gemmell, J.B., and Herzig, P.M., 1995. PACMANUS: an active seafloor hydrothermal field on siliceous volcanic rocks in the Eastern Manus Basin, Papua New Guinea. In Mauk, J.L., and St. George, J.D. (Eds.), *Proc. 1995 Pac. Rim Congress*, Australas. Inst. Min. Metall., Melbourne, 49–54.
- Binns, R.A., Parr, J.M., Waters, J.S., Gemmell, J.B., Moss, R., Scott, S.D., Naka, J., Charlou, J.-L., Gena, K., and Herzig, P.M., 1996a. Actively-forming sulfide deposits at the PACMANUS hydrothermal field, Eastern Manus Basin, Papua New Guinea. *Eos, Trans. Am. Geophys. Union*, 77:W115–116.
- Binns, R.A., and Scott, S.D., 1993. Actively forming polymetallic sulfide deposits associated with felsic volcanic rocks in the eastern Manus back-arc basin, Papua New Guinea. *Econ. Geol.*, 88:2226–2236.
- Binns, R.A., Scott, S.D., and Gemmell, J.B., 1997a. Modern analogue of a mineral field: Sea-floor hydrothermal activity hosted by felsic volcanic rocks in the Eastern Manus Basin, Papua New Guinea. *Soc. Econ. Geol., Neves Corvo Field Conf.*, Abstr. Program, 33.
- Binns, R.A., Scott, S.D., Gemmell, J.B., Crook, K.A.W.C., and Shipboard Party, 1997b. The SuSu Knolls hydrothermal field, Eastern Manus Basin, Papua New Guinea. *Eos, Trans. Am. Geophys. Union*, 78:F772.
- Binns, R.A., Waters, J.C., Carr, G.R., and Whitford, D.J., 1996b. A submarine andesite-rhyodacite lineage of arc affinity, Pual Ridge, eastern Manus back-arc basin, Papua New Guinea. *Eos, Trans. Am. Geophys. Union*, 77:119–120.
- Boynnton, W.V., 1984. Cosmochemistry of the rare earth elements: meteorite studies. In Henderson, P. (Ed.), *Rare Earth Element Geochemistry*: New York (Elsevier), 63–114.
- Butterfield, D.A., McDuff, R.E., Franklin, J., and Wheat, C.G., 1994. Geochemistry of hydrothermal vent fluids from Middle Valley, Juan de Fuca Ridge. In Mottl, M.J., Davis, E.E., Fisher, A.T., and Slack, J.F. (Eds.), *Proc. ODP, Sci. Results*, 139: College Station, TX (Ocean Drilling Program), 395–410.
- Cragg, B.A., Summit, M., and Parkes, R.J., 2000. Bacterial profiles in a sulfide mound (Site 1035) and an area of active fluid venting (Site 1036) in hot hydrothermal sediments from Middle Valley (northwest Pacific). In Zierenberg, R.A., Fouquet, Y., Miller, D.J., and Normark, W.R. (Eds.), *Proc. ODP, Sci. Results*, 169: College Station, TX (Ocean Drilling Program), 1–18. doi:10.2973/odp.proc.sr.169.105.2000
- Davis, E.E., Mottl, M.J., Fisher, A.T., et al., 1992. *Proc. ODP, Init. Repts.*, 139: College Station, TX (Ocean Drilling Program).
- Duckworth, R.C., Fallick, A.E., and Rickard, D., 1994. Mineralogy and sulfur isotopic composition of the Middle Valley massive sulfide deposit, northern Juan de Fuca Ridge. In Mottl, M.J., Davis, E.E., Fisher, A.T., and Slack, J.F. (Eds.), *Proc. ODP, Sci. Results*, 139: College Station, TX (Ocean Drilling Program), 373–385.
- Fouquet, Y., Zierenberg, R.A., Miller, D.J., et al., 1998. *Proc. ODP, Init. Repts.*, 169: College Station, TX (Ocean Drilling Program). [HTML]
- Hannington, M.D., Galley, A.G., Herzig, P.M., and Petersen, S., 1998. Comparison of the TAG mound and stockwork complex with Cyprus-type massive sulfide deposits. In Herzig, P.M., Humphris, S.E., Miller, D.J., and Zierenberg, R.A. (Eds.), *Proc.*

- ODP, Sci. Results*, 158: College Station, TX (Ocean Drilling Program), 389–415. [PDF]
- Herzig, P.M., and Hannington, M.D., 2000. Polymetallic massive sulfides and gold mineralization at mid-ocean ridges and in subduction-related environments. In Cronan, D.S. (Ed.), *Handbook of Marine Mineral Deposits*: Boca Raton (CRC Press), 347–368.
- Herzig, P.M., Humphris, S.E., Miller, D.J., and Zierenberg, R.A. (Eds.), 1998. *Proc. ODP, Sci. Results*, 158: College Station, TX (Ocean Drilling Program). [HTML]
- Herzig, P.M., Petersen, S., and Hannington, M.D., 1998. Geochemistry and sulfur-isotopic composition of the TAG hydrothermal mound, Mid-Atlantic Ridge, 26°N. In Herzig, P.M., Humphris, S.E., Miller, D.J., and Zierenberg, R.A. (Eds.), *Proc. ODP, Sci. Results*, 158: College Station, TX (Ocean Drilling Program), 47–70. [PDF]
- Honnorez, J.J., Alt, J.C., and Humphris, S.E., 1998. Vivisection and autopsy of active and fossil hydrothermal alterations of basalt beneath and within the TAG hydrothermal mound. In Herzig, P.M., Humphris, S.E., Miller, D.J., and Zierenberg, R.A. (Eds.), *Proc. ODP, Sci. Results*, 158: College Station, TX (Ocean Drilling Program), 231–254. [PDF]
- Humphris, S.E., Alt, J.C., Teagle, D.A.H., and Honnorez, J.J., 1998. Geochemical changes during hydrothermal alteration of basement in the stockwork beneath the active TAG hydrothermal mound. In Herzig, P.M., Humphris, S.E., Miller, D.J., and Zierenberg, R.A. (Eds.), *Proc. ODP, Sci. Results*, 158: College Station, TX (Ocean Drilling Program), 255–276. [PDF]
- Humphris, S.E., Herzig, P.M., Miller, D.J., Alt, J.C., Becker, K., Brown, D., Brüggmann, G., Chiba, H., Fouquet, Y., Gemmell, J.B., Guerin, G., Hannington, M.D., Holm, N.G., Honnorez, J.J., Itturino, G.J., Knott, R., Ludwig, R., Nakamura, K., Petersen, S., Reysenbach, A.-L., Rona, P.A., Smith, S., Sturz, A.A., Tivey, M.K., and Zhao, X., 1995. The internal structure of an active sea-floor massive sulphide deposit. *Nature (London, U. K.)*, 377(6551):713–716. doi:10.1038/377713a0
- Humphris, S.E., Herzig, P.M., Miller, D.J., et al., 1996. *Proc. ODP, Init. Repts.*, 158: College Station, TX (Ocean Drilling Program).
- James, R.H., Duckworth, R.C., Palmer, M.R., and the ODP Leg 169 Shipboard Scientific Party, 1998. Drilling of sediment-hosted massive sulphide deposits at the Middle Valley and Escanaba Trough spreading centres: ODP Leg 169. In Mills, R.A., and Harrison, K. (Eds.), *Modern Ocean Floor Processes and the Geological Record*. Spec. Publ.—Geol. Soc. London, 148:177–199.
- Johnson, R.W., 1976. Late Cainozoic volcanism and plate tectonics at the southern margin of the Bismarck Sea, Papua New Guinea. In Johnson, R.W. (Ed.), *Volcanism in Australasia*: Amsterdam (Elsevier), 101–116.
- Krasnov, S., Stepanova, T., and Stepanov, M., 1994. Chemical composition and formation of a massive sulfide deposit, Middle Valley, northern Juan de Fuca Ridge (Site 856). In Mottl, M.J., Davis, E.E., Fisher, A.T., and Slack, J.F. (Eds.), *Proc. ODP, Sci. Results*, 139: College Station, TX (Ocean Drilling Program), 353–372.
- Kurnosov, V., Murdmaa, I., Rosanova, T., Kashintzev, G., Eroshchev-Shak, V., and Krasnov, S., 1994. Mineralogy of hydrothermally altered sediments and igneous rocks at Sites 856–858, Middle Valley, Juan de Fuca Ridge, Leg 139. In Mottl, M.J., Davis, E.E., Fisher, A.T., and Slack, J.F. (Eds.), *Proc. ODP, Sci. Results*, 139: College Station, TX (Ocean Drilling Program), 113–131.
- Lee, K.-Y. (Ed.), 2000. A geochemical study for the submarine hydrothermal mineralization, II. Korean Ocean Research and Development Institute Rept. PE99758-00-1240-7.
- Mottl, M.J., Davis, E.E., Fisher, A.T., and Slack, J.F. (Eds.), 1994. *Proc. ODP, Sci. Results*, 139: College Station, TX (Ocean Drilling Program).
- Reysenbach, A.-L., Holm, N.G., Hershberger, K., Prieur, D., and Jeanthon, C., 1998. In search of a subsurface biosphere at a slow-spreading ridge. In Herzig, P.M., Humphris, S.E., Miller, D.J., and Zierenberg, R.A. (Eds.), *Proc. ODP, Sci. Results*, 158: College Station, TX (Ocean Drilling Program), 355–360. [PDF]

- Shipboard Scientific Party, 2002a. Leg 193 summary. *In* Binns, R.A., Barriga, F.J.A.S., Miller, D.J., et al., *Proc. ODP, Init. Repts.*, 193: College Station, TX (Ocean Drilling Program), 1–84. doi:10.2973/odp.proc.ir.193.101.2002
- Shipboard Scientific Party, 2002b. Site 1188. *In* Binns, R.A., Barriga, F.J.A.S., Miller, D.J., et al., *Proc. ODP, Init. Repts.*, 193: College Station, TX (Ocean Drilling Program), 1–305. doi:10.2973/odp.proc.ir.193.103.2002
- Shipboard Scientific Party, 2002c. Site 1189. *In* Binns, R.A., Barriga, F.J.A.S., Miller, D.J., et al., *Proc. ODP, Init. Repts.*, 193: College Station, TX (Ocean Drilling Program), 1–259. doi:10.2973/odp.proc.ir.193.104.2002
- Shipboard Scientific Party, 2002d. Site 1190. *In* Binns, R.A., Barriga, F.J.A.S., Miller, D.J., et al., *Proc. ODP, Init. Repts.*, 193: College Station, TX (Ocean Drilling Program), 1–15. doi:10.2973/odp.proc.ir.193.105.2002
- Stuart, F.M., Ellam, R.M., and Duckworth, R.C., 1999. Metal sources in the Middle Valley massive sulphide deposit, northern Juan de Fuca Ridge: Pb isotope constraints. *Chem. Geol.*, 153(1–4):213–225. doi:10.1016/S0009-2541(98)00148-X
- Summit, M., Peacock, A., Ringelberg, D., White, D.C., and Baross, J.A., 2000. Phospholipid fatty acid-derived microbial biomass and community dynamics in hot, hydrothermally influenced sediments from Middle Valley, Juan de Fuca Ridge. *In* Zierenberg, R.A., Fouquet, Y., Miller, D.J., and Normark, W.R. (Eds.), *Proc. ODP, Sci. Results*, 169: College Station, TX (Ocean Drilling Program), 1–19. doi:10.2973/odp.proc.sr.169.117.2000
- Taylor, B., 1979. Bismarck Sea: evolution of a back-arc basin. *Geology*, 7(4):171–174. doi:10.1130/0091-7613(1979)7<171:BSEOAB>2.0.CO;2
- Tivey, M.K., Mills, R.A., and Teagle, D.A.H., 1998. Temperature and salinity of fluid inclusions in anhydrite as indicators of seawater entrainment and heating in the TAG active mound. *In* Herzig, P.M., Humphris, S.E., Miller, D.J., and Zierenberg, R.A. (Eds.), *Proc. ODP, Sci. Results*, 158: College Station, TX (Ocean Drilling Program), 179–190. [PDF]
- Waters, J.C., and Binns, R.A., 1998. Contrasting styles of felsic submarine volcanism, eastern Manus Basin, Papua New Guinea. *Abstr.—Geol. Soc. Aust.*, 49:459.
- Waters, J.C., Binns, R.A., and Naka, J., 1996. Morphology of submarine felsic volcanic rocks on Pual Ridge, Eastern Manus Basin, Papua New Guinea. *Eos, Trans. Am. Geophys. Union*, 77:W120.
- Woodhead, J.D., and Johnson, R.W., 1993. Isotopic and trace-element profiles across the New Britain island arc, Papua New Guinea. *Contrib. Mineral. Petrol.*, 113(4):479–491. doi:10.1007/BF00698317
- Yang, K., and Scott, S.D., 2002. Magmatic degassing of volatiles and ore minerals into a hydrothermal system on the modern sea floor of the eastern Manus back-arc basin, western Pacific. *Econ. Geol.*, 97(5):1079–1100. doi:10.2113/97.5.1079
- Zierenberg, R.A., Fouquet, Y., Miller, D.J., Bahr, J.M., Baker, P.A., Bjerkgård, T., Brunner, C.A., Duckworth, R.C., Gable, R., Gieskes, J., Goodfellow, W.D., Gröschel-Becker, H.M., Guèrin, G., Ishibashi, J., Iturrino, G., James, R.H., Lackschewitz, K.S., Marquez, L.L., Nehlig, P., Peter, J.M., Rigsby, C.A., Schultheiss, P., Shanks, W.C., III, Simoneit, B.R.T., Summit, M., Teagle, D.A.H., Urvat, M., and Zuffa, G.G., 1998. The deep structure of a sea-floor hydrothermal deposit. *Nature (London, U. K.)*, 392(6675):485–488. doi:10.1038/33126
- Zierenberg, R.A., Fouquet, Y., Miller, D.J., and Normark, W.R. (Eds.), 2000. *Proc. ODP, Sci. Results*, 169: College Station, TX (Ocean Drilling Program). doi:10.2973/odp.proc.sr.169.2000

**Figure F1. A.** Location and geologic setting of the PACMANUS hydrothermal field (modified from Shipboard Scientific Party, 2002a). Seafloor bathymetry basemap from [www.ngdc.noaa.gov/mgg/image/2minsurface/1350/00N135E.jpg](http://www.ngdc.noaa.gov/mgg/image/2minsurface/1350/00N135E.jpg). Inactive (dashed orange line with teeth on overriding plate) and active (red solid line with teeth on overriding plate) subduction zones encompass the Manus spreading center between Papua New Guinea and New Britain to the south and New Ireland to the north. The PACMANUS area lies between transform faults east of the Manus spreading center. Sites of nearby active volcanism are marked by orange serrated circles. Thick blue arrows indicate plate motions, and the orange bars spanning Woodlark Basin indicate spreading segments. (Continued on next page.)

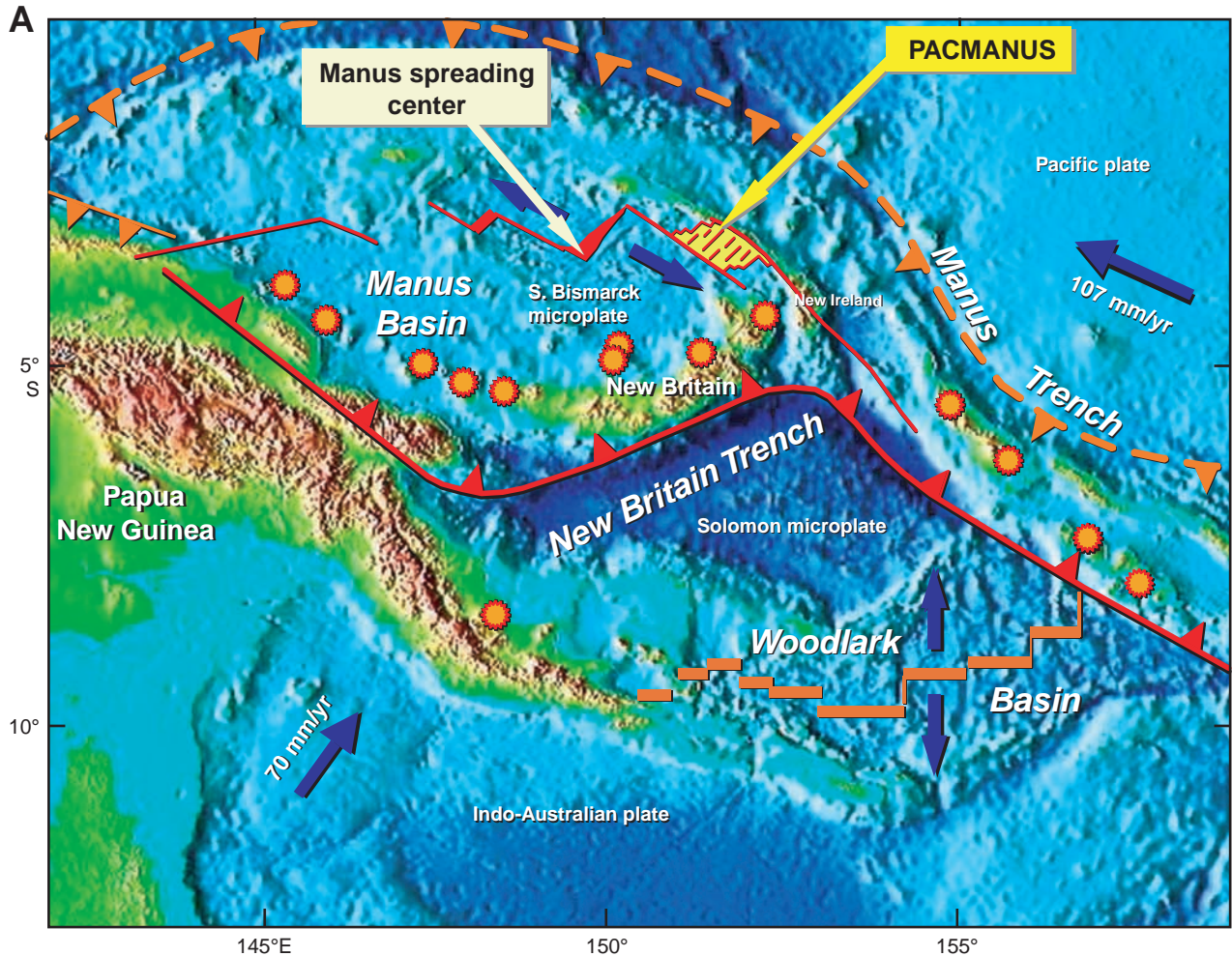
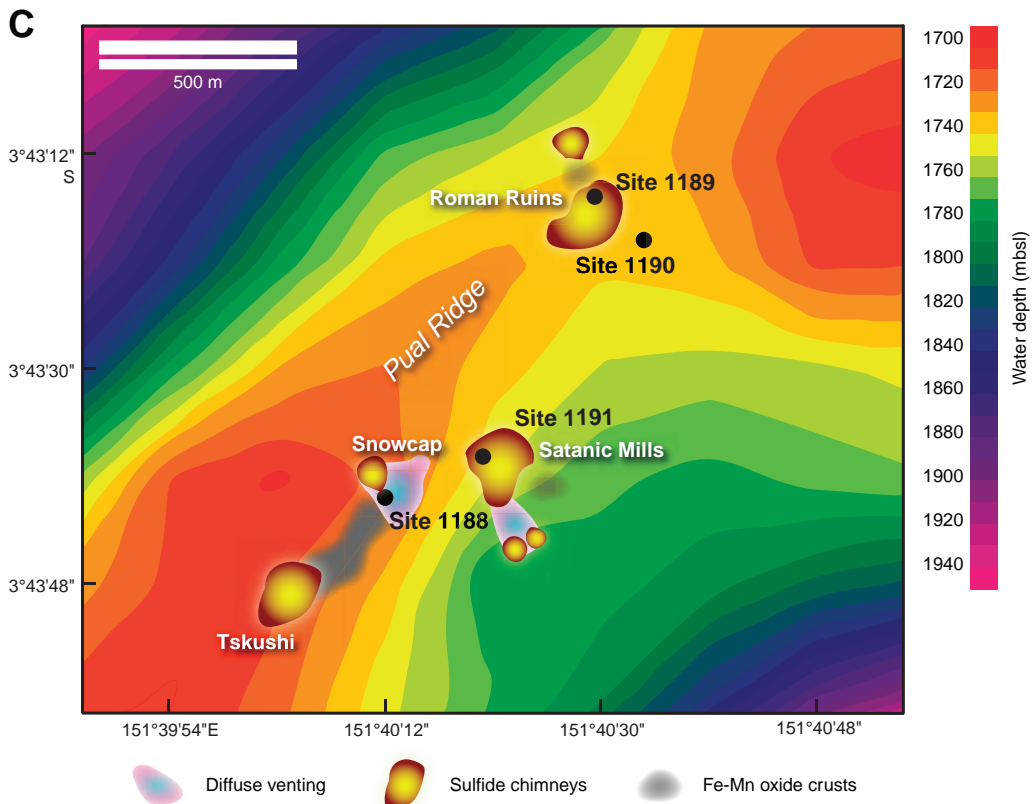
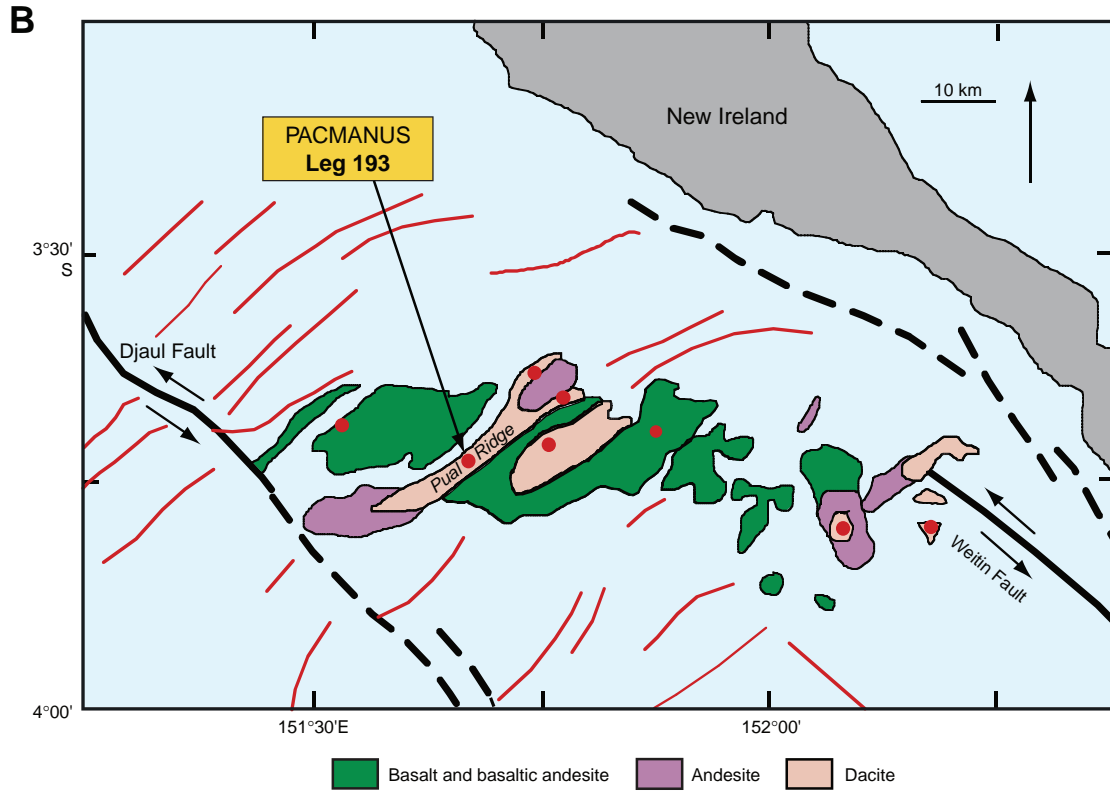
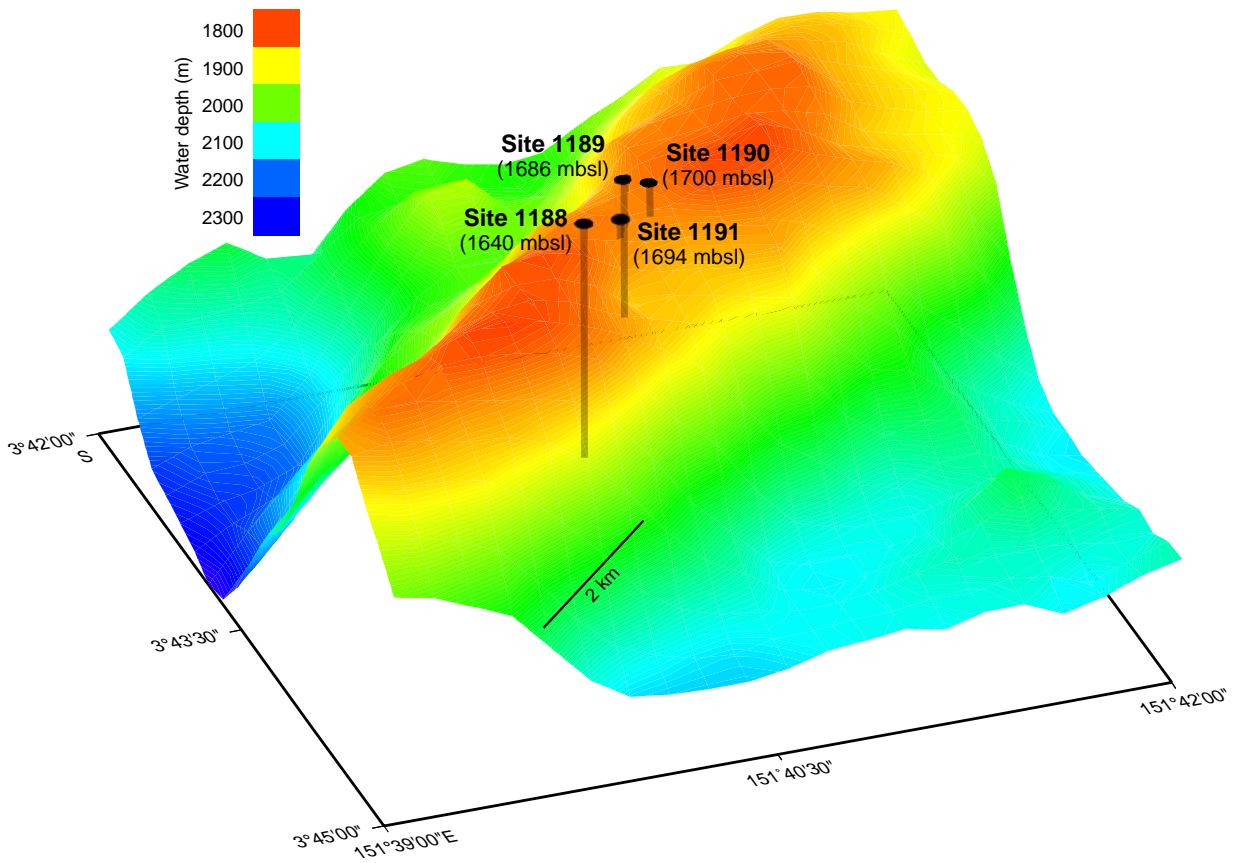


Figure F1 (continued). B. Seafloor geology of PACMANUS area (yellow shaded area in Fig. F1A, p. 13) in the Eastern Manus Basin (modified from Binns, Barriga, Miller, et al., 2002). Red circles = locations of known hydrothermal sites, red lines = extensional fault scarps. C. Active hydrothermal areas and drill sites at PACMANUS.



**Figure F2.** Three-dimensional shaded-relief image (10× vertical exaggeration) along Pual Ridge (bathymetry data from Lee, 2000). Image shows the relative locations and depth to seafloor of Sites 1188 (Snowcap), 1189 (Roman Ruins), 1190 (reference site), and 1191 (Satanic Mills). Shaded lines beneath holes indicate relative depth of penetration at each site.



**Figure F3.** A. Euhedral clinopyroxene phenocryst with flow-oriented plagioclase microlites in the groundmass of Sample 193-1188A-3R-1, 0 cm. Cross-polarized light, field of view = 0.7 mm. B. Euhedral plagioclase and clinopyroxene phenocrysts from Sample 193-1188A-2R-1, 11 cm. Cross-polarized light, field of view = 0.7 mm. C. Melt inclusions in plagioclase from Sample 193-1188A-2R-1, 11 cm. Cross-polarized light, field of view = 1.25 mm. D. Subhedral magnetite microphenocrysts (opaque) in flow-aligned plagioclase microlite-bearing glassy groundmass. Sample 193-1188A-2R-1, 11 cm. Plane-polarized light, field of view = 0.7 mm.

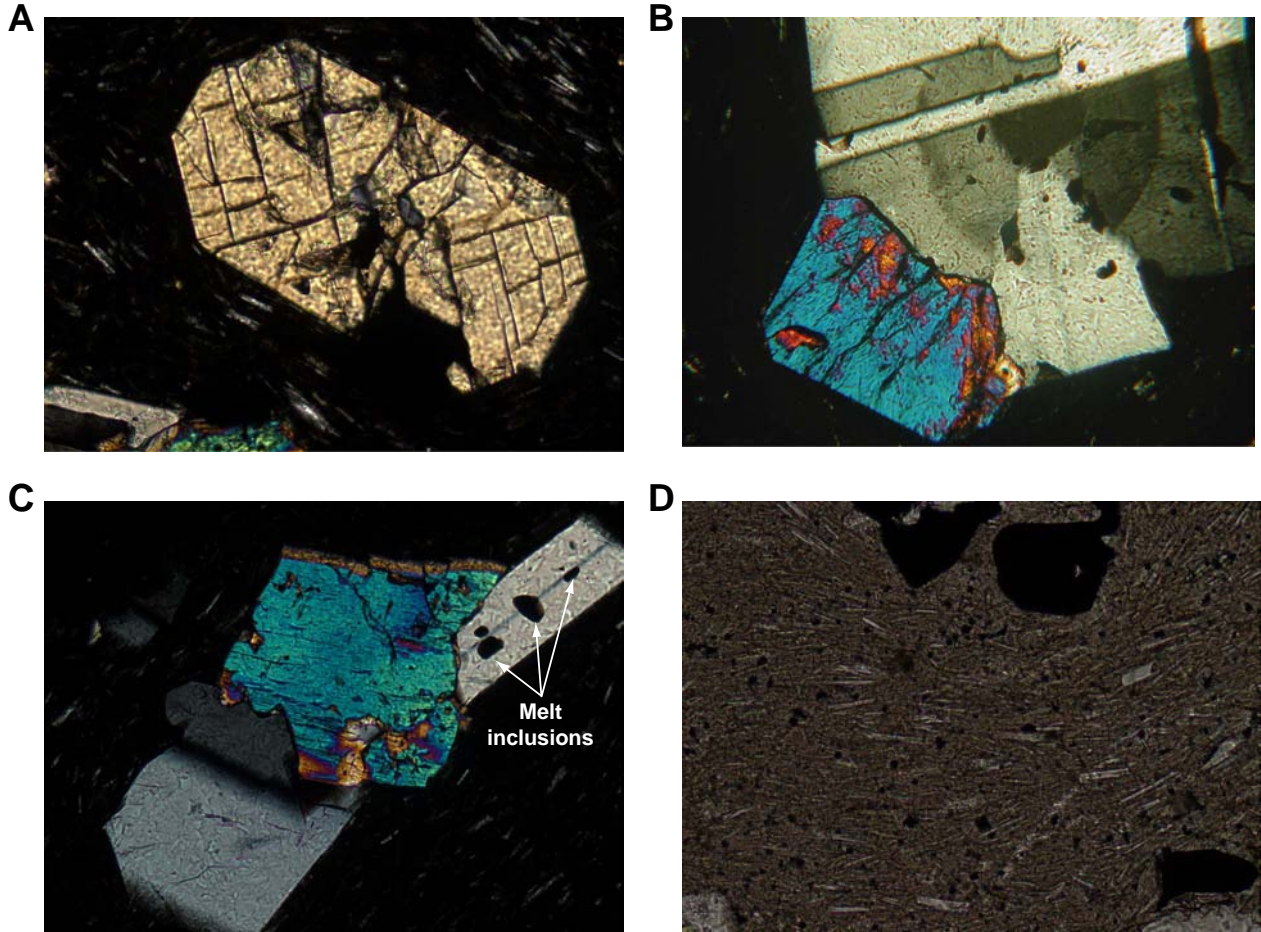


Figure F4. A. Jackstraw-textured plagioclase microlites in glassy groundmass from Sample 193-1189A-1R-1, 10 cm. Plane-polarized light, field of view = 0.7 mm. B. Resorbed plagioclase phenocrysts from Sample 193-1189B-6R-1, 36 cm. Cross-polarized light, field of view = 1.4 mm.

A



B

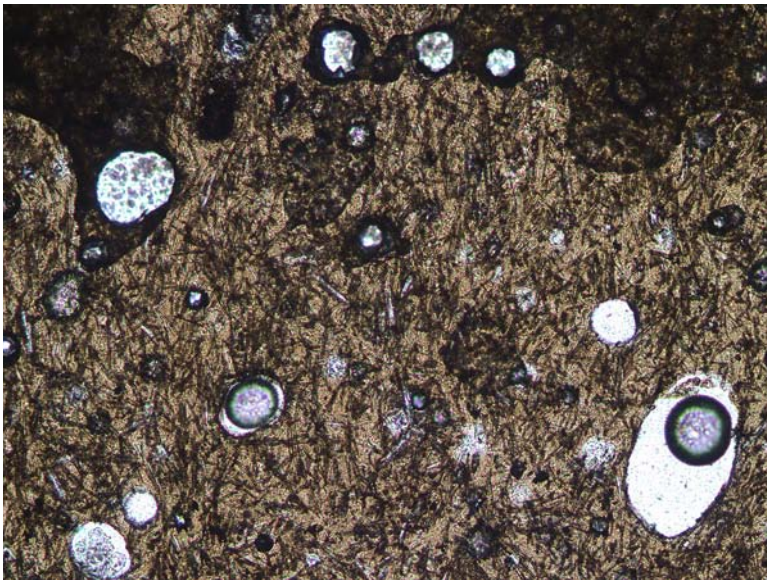
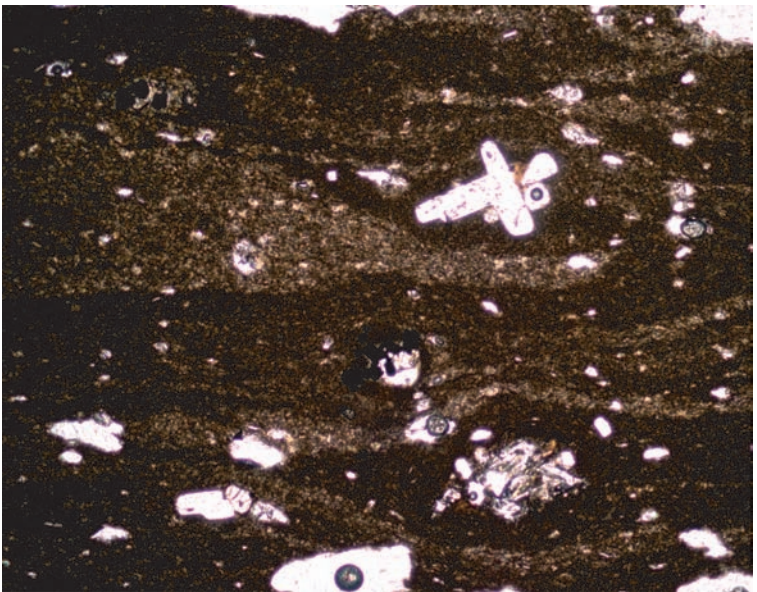


Figure F5. A. Rounded plagioclase and clinopyroxene phenocrysts from Sample 193-1190A-2R-1, 40 cm. Circular feature in lower center of image is a bubble in the epoxy. Plane-polarized light, field of view = 1.4 mm. B. Flow banding in Sample 193-1190C-1R-1, 16 cm. Plane-polarized light, field of view = 1.4 mm.

A



B



**Figure F6.** Euhedral plagioclase and clinopyroxene phenocrysts in Sample 193-1191A-3R-1, 12 cm. Cross-polarized light, field of view = 0.7 mm.

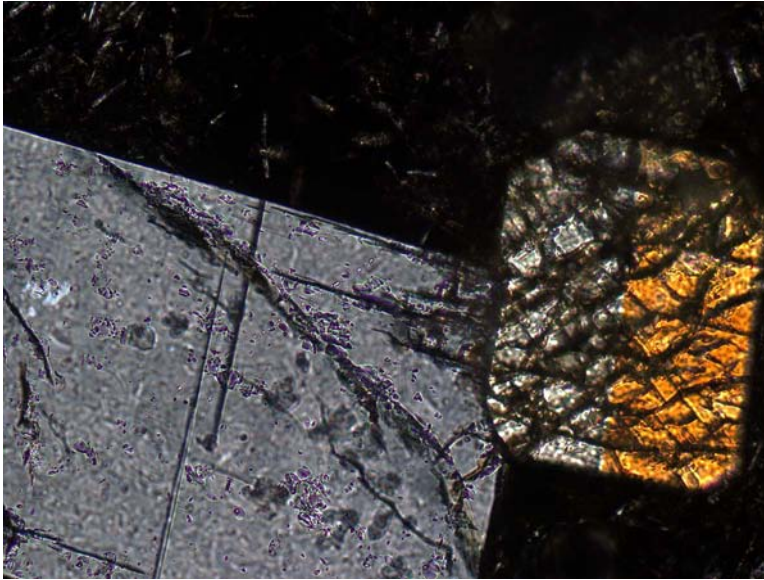


Figure F7. Bulk rock compositions of all samples reported in this study plotted as total alkali vs. silica. Shaded field is the compilation of bulk rock compositions and matrix glass compositions of samples from Eastern Manus Basin presented in Yang and Scott, 2002. Solid symbols = this study, open symbols = ship-board analyses.

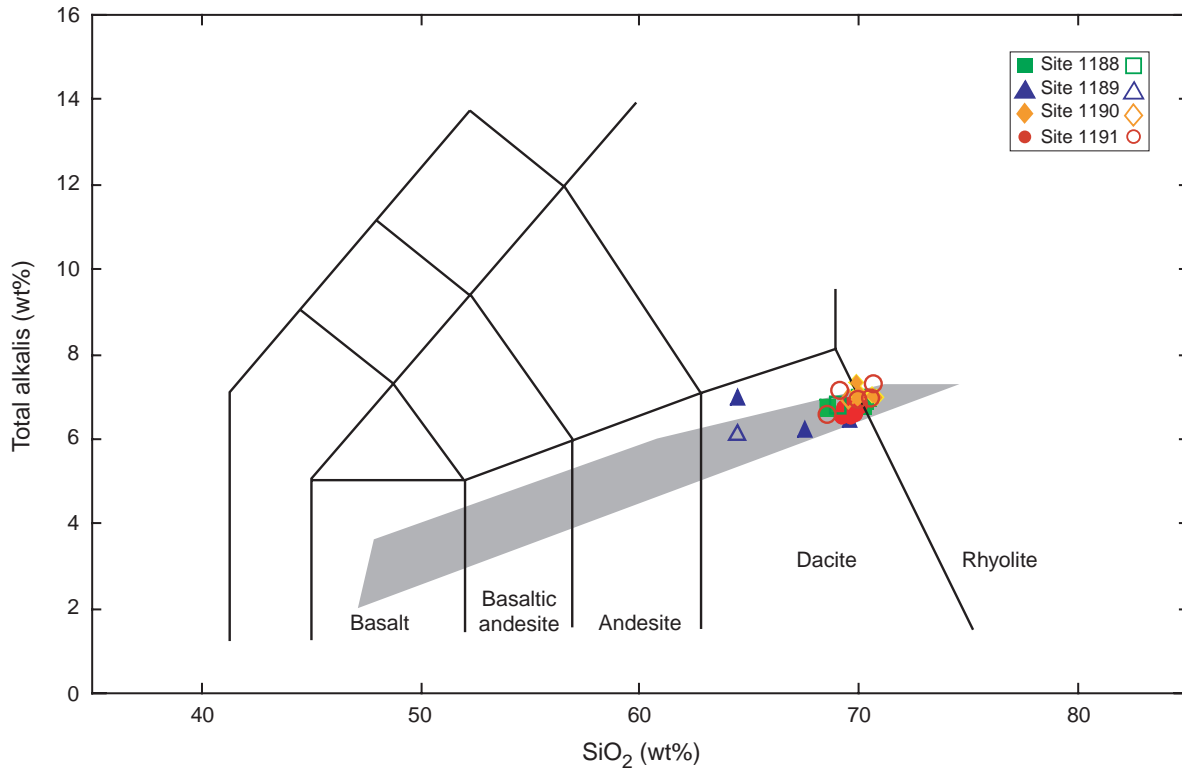
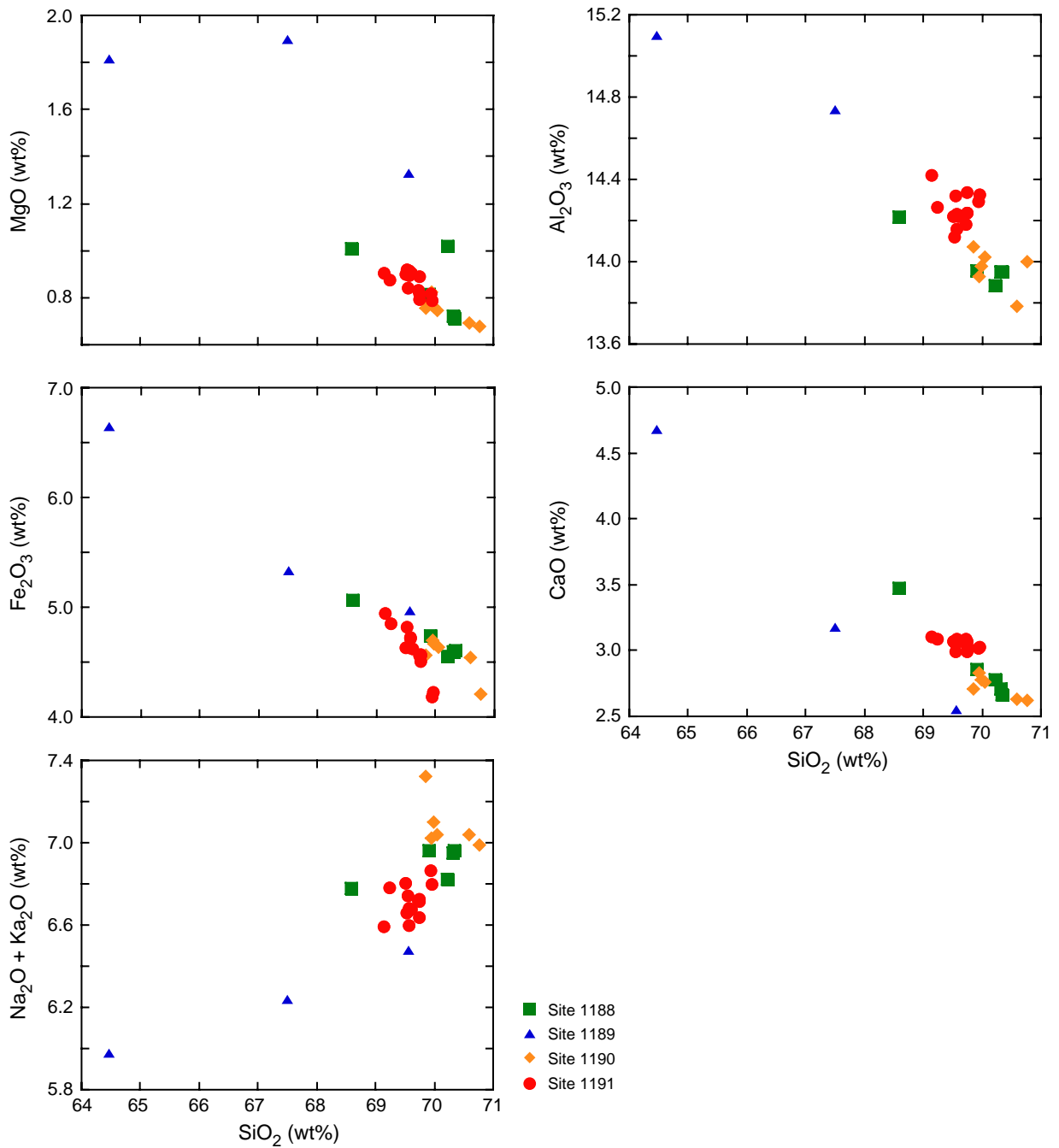


Figure F8. Covariation diagrams of SiO<sub>2</sub> relative to MgO, Al<sub>2</sub>O<sub>3</sub>, Fe<sub>2</sub>O<sub>3</sub> (total Fe), CaO, and Na<sub>2</sub>O + K<sub>2</sub>O.

**Figure F9. A.** Covariation diagram of  $\text{TiO}_2$  vs. Zr in fresh lavas from the crest of Pual Ridge showing a distinct fractionation trend. The sample with anomalously low Zr (106 ppm) at 0.5 wt%  $\text{TiO}_2$  has a sample taken from 2 cm away with 125 ppm Zr and 0.5 wt%  $\text{TiO}_2$  that plots on the best-fit trend line. **B.** Covariation diagram of  $\text{SiO}_2$  vs. Ti/Zr in fresh lavas from the crest of Pual Ridge showing a fractionation trend. Elevated Ti/Zr may be a result of incipient alteration. Solid symbols = this study, open symbols = shipboard analyses.

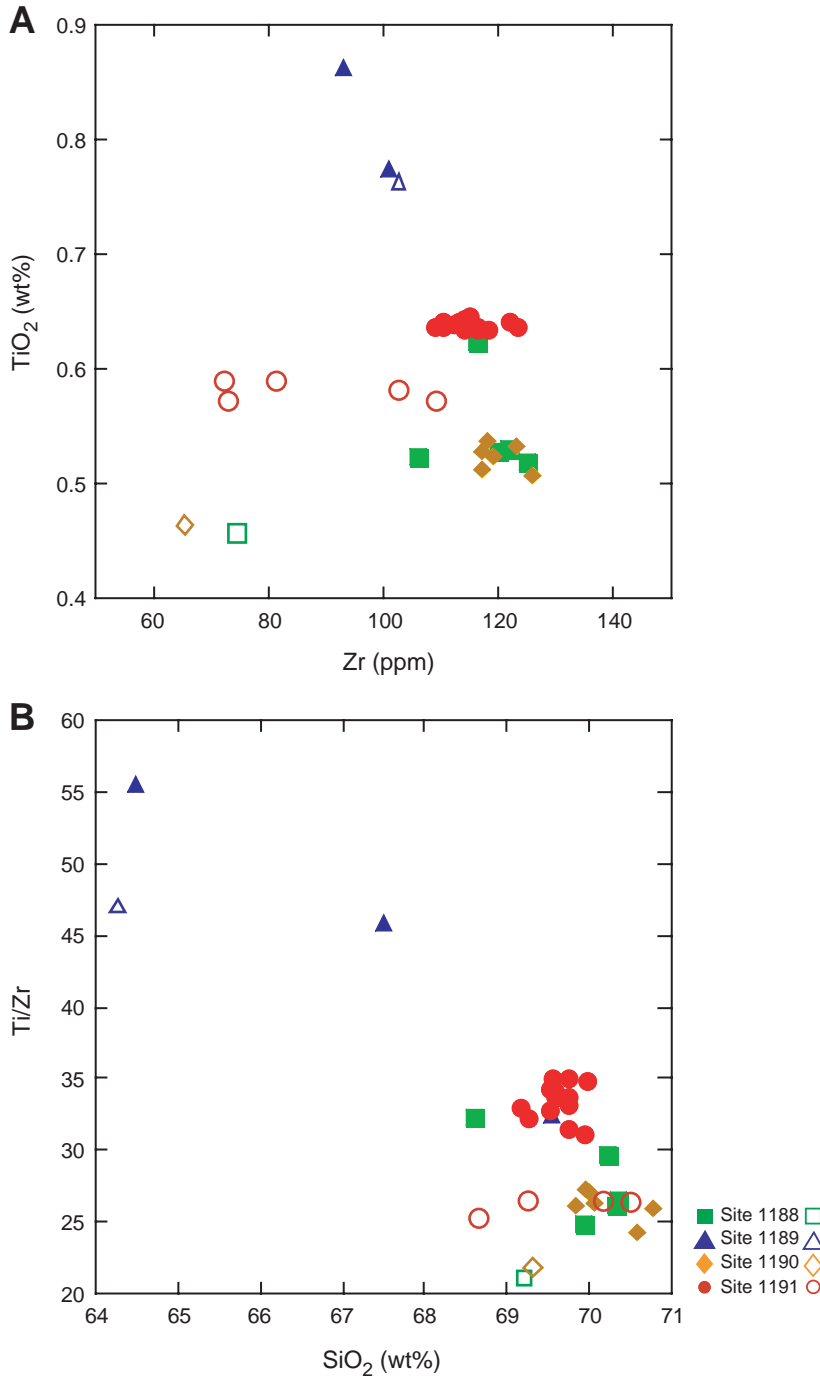


Figure F10. Chondrite-normalized rare earth element spider diagram patterns of fresh lava samples from all four sites cored during Leg 193. The tight cluster suggests that these lavas were likely derived from a common parent despite small-volume flows separated by as much as several hundred meters along the crest of the ridge.

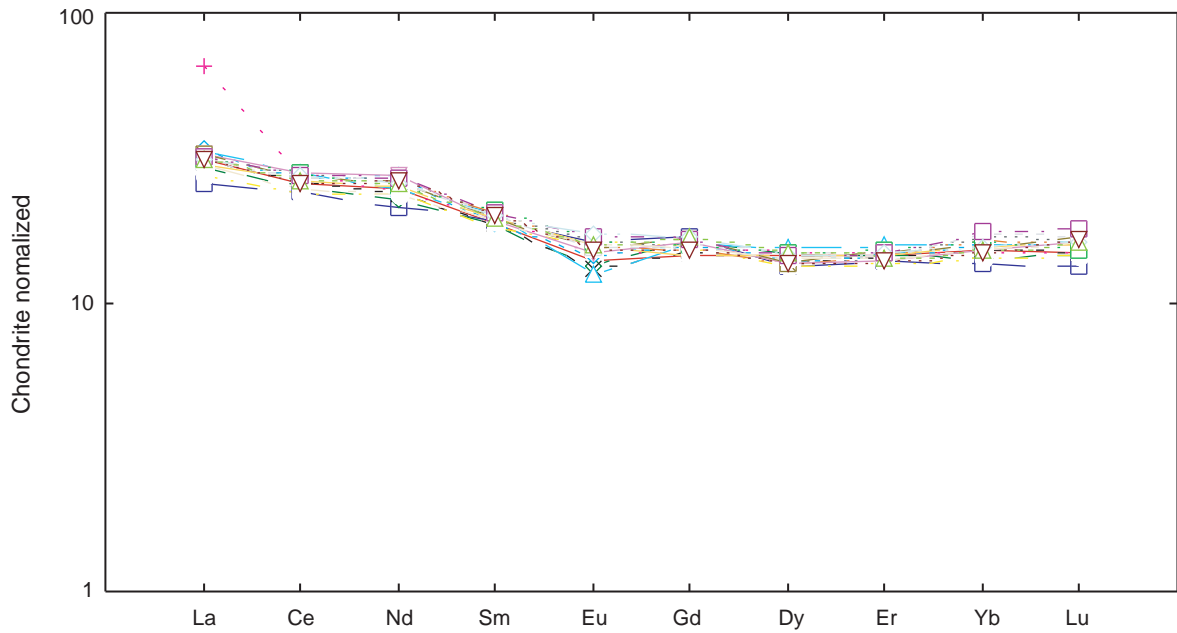


Figure F11. Covariation diagrams of Eu/Eu\* relative to SiO<sub>2</sub>, CaO, and Sr.

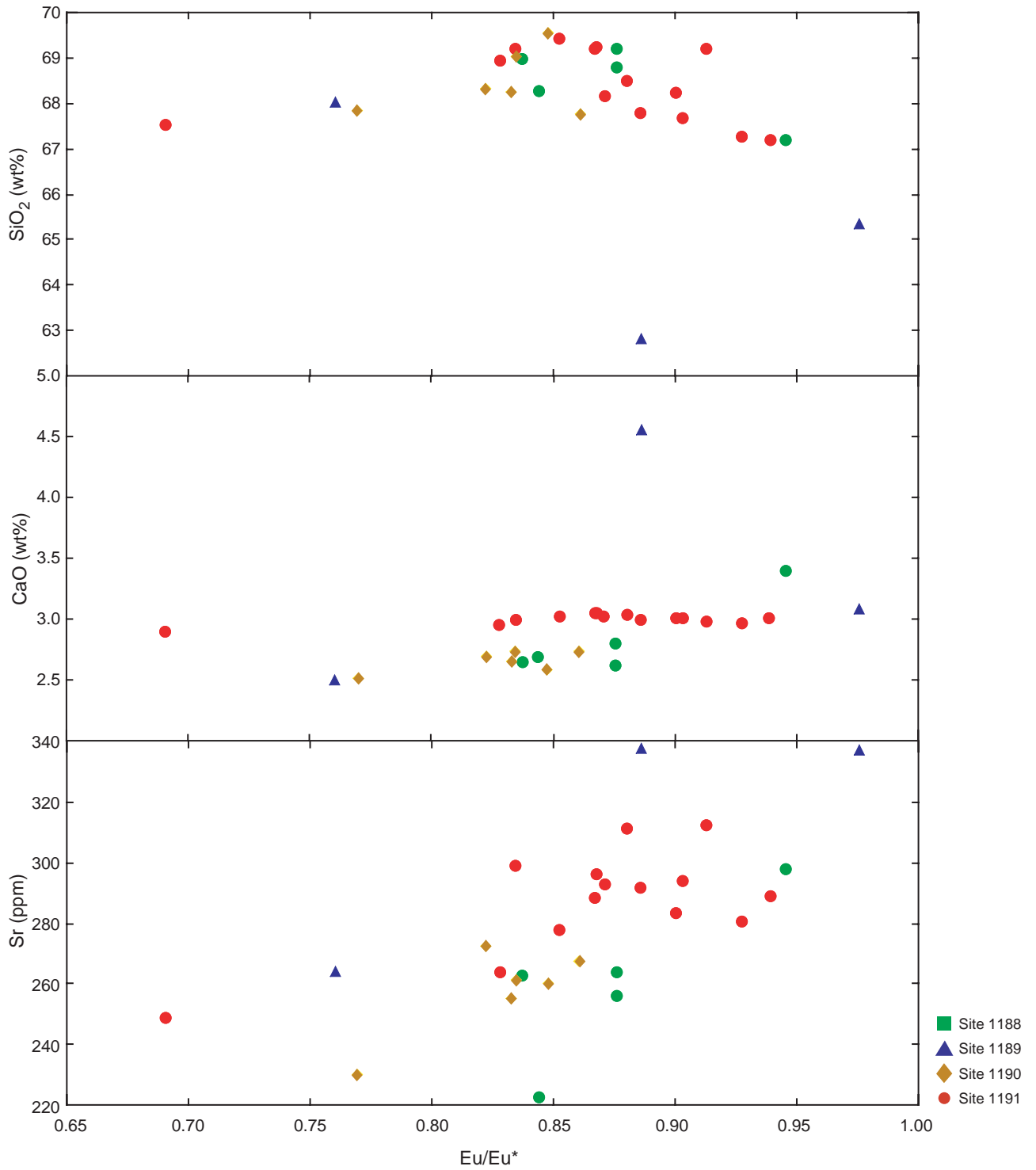


Figure F12. A. Range of anorthite content in plagioclase analyses. Compiled from core to rim transects across single crystals and individual crystal analyses. B. Representative pyroxene compositions from Sites 1188 (green), 1190 (orange), and 1191 (red).

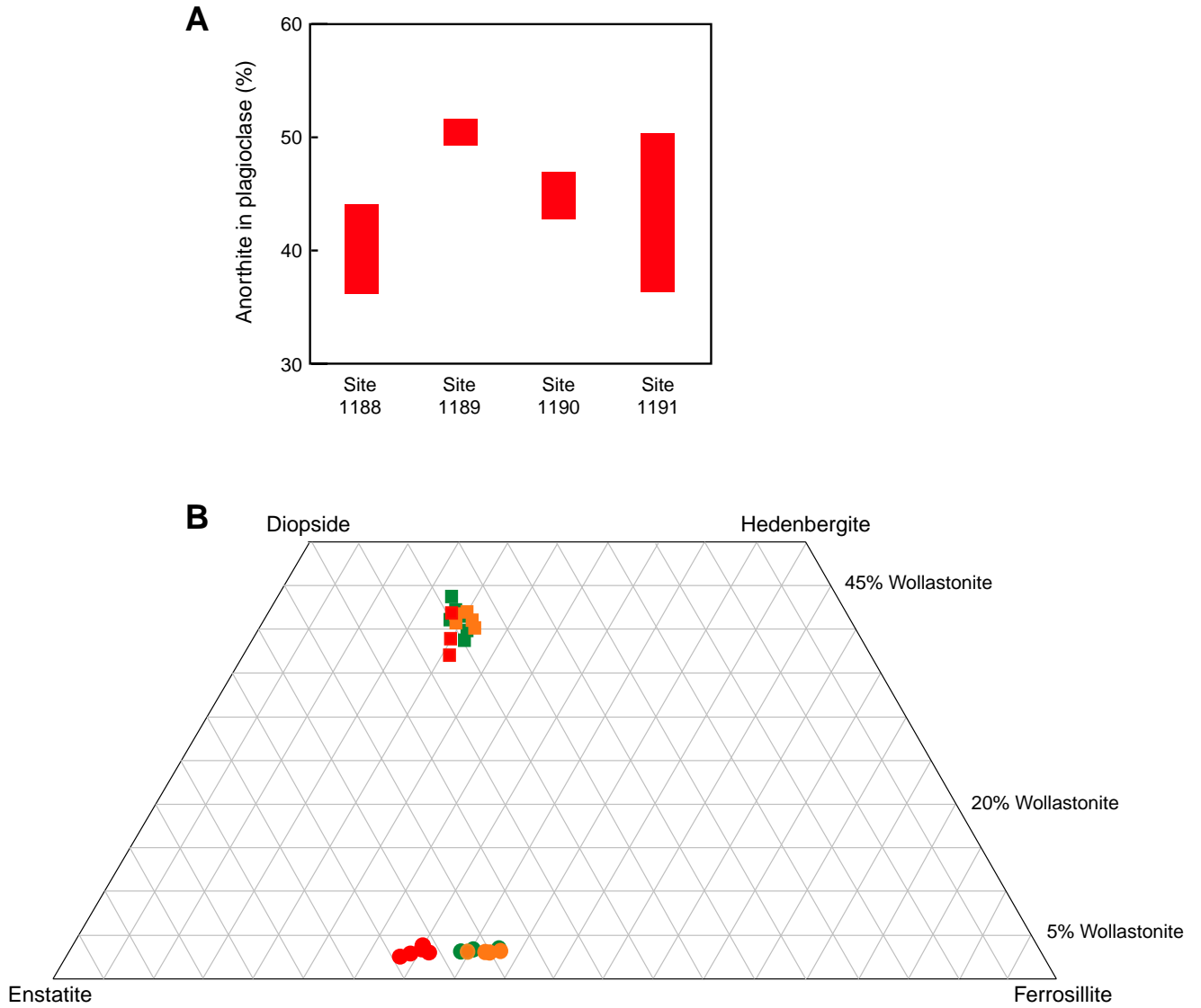




Table T1 (continued).

Core, section, interval (cm)	Depth (mbsf)	Phenocrysts	Analyses	Anhydrous (%)					Trace elements (ppm)																
				MnO	Na <sub>2</sub> O	K <sub>2</sub> O	P <sub>2</sub> O <sub>5</sub>	Total	Ba	Cu	Pb	Zn	Co	Ga	Hf	Mo	Nb	Ni	Rb	Sc	Sr	Th			
193-1188A-																									
2R-1, 10	9.7	Moderately phyric	JM	0.11	4.82	2.15	0.12	100	379	12.8	0.5	22	4.8	15.9	4.1	0.3	2.7	1.7	32.3	11	256.1	1.8			
2R-1, 18	9.78	Moderately phyric	HP	0.11	4.80	2.02	0.10	100	381	25	10	103	5.1	17.4	3.9	4.96	1.56	15	33	10.7	223	2.16			
2R-1, 20	9.8	Moderately phyric	JM	0.11	4.78	2.18	0.11	100	378	15.7	1.4	26	5.2	16.4	3.9	0.2	1.8	11.1	31.6	11	264	1.4			
7R-1, 6	48.26	Moderately phyric	JM	0.11	4.80	2.15	0.11	100	383	14.2	1.3	28	3.8	15.5	3.8	0.3	2.1	1.8	31.7	11	263	1.8			
5R-1, 12	33.72	Sparsely phyric	JM	0.11	4.75	2.03	0.14	100	371	8	12.5	10	5.4	17.4	4.1	0.1	2.2	1.2	30.3	12	298.3	0.9			
193-1191A-																									
1R-1, 38	0.38	Aphyric	JM	0.11	4.93	1.74	0.13	100	335	11.3	1.5	35	4.8	15.7	3.4	0.8	1.8	0.4	27.2	11	280.8	1.3			
1R-1, 61	0.61	Aphyric	JM	0.11	5.00	1.68	0.13	100	345	14.7	1.7	33	4.7	18.5	3.7	0.9	1.9	0.6	21.14	12	288.8	1.1			
1R-1, 64	0.64	Aphyric	HP	0.11	4.93	1.78	0.13	100	354	29	4	70	5.3	18.5	3.6	1.88	1.51	4	28	14.0	264	2.34			
1R-1, 75	0.75	Aphyric	HP	0.12	4.95	1.79	0.14	100	331	22	6	98	5.3	16.8	4.0	2.66	1.43	371	28	15.2	249	2.18			
1R-1, 77	0.77	Sparsely phyric	JM	0.11	4.88	1.72	0.13	100	344	8.6	1	24	4.6	16.5	3.5	0.2	2	2.3	26.7	11	289.2	1			
2R-1, 12	9.52	Sparsely phyric	JM	0.11	4.89	1.71	0.12	100	355	25.1	6.2	42	4.9	16.8	4	0.9	1.7	0.8	29.1	12	293.4	0.9			
2R-1, 76	10.16	Aphyric	JM	0.11	4.88	1.84	0.11	100	350	17.9	3.5	38	4.6	17	3.4	1	1.6	0.8	20.8	12	296.5	0.8			
2R-1, 128	10.68	Sparsely phyric	JM	0.11	4.88	1.76	0.12	100	360	12.9	2.5	33	4.8	15.9	3.4	0.9	1.7	0.9	21.7	12	277.9	1			
2R1, 145	10.83	Sparsely phyric	JM	0.10	5.05	1.82	0.13	100	365	11.6	5.5	62	5.4	16.4	3.3	0.7	2	0.9	23.4	12	312.5	1.4			
2R-2, 22	11.12	Sparsely phyric	JM	0.11	5.02	1.78	0.11	100	368	12.8	3.1	43	4.5	16.5	3.4	0.7	1.6	0.6	21.7	11	299.1	1.4			
2R-2, 88	11.78	Sparsely phyric	JM	0.11	5.02	1.78	0.12	100	359	17.7	2.9	39	5.2	16.6	3.5	1.2	2.3	0.9	22.9	12	292.3	1.1			
2R-2, 90	11.8	Aphyric	JM	0.11	4.85	1.83	0.13	100	361	16.5	2.9	39	4.4	16.7	3.6	1.2	1.8	1	26	12	283.8	1.4			
3R-1, 18	14.88	Sparsely phyric	JM	0.12	4.99	1.79	0.12	100	345	4	0.3	11	4.9	15.6	3.5	0.1	1.8	0.6	29.8	11	294	1.6			
3R-1, 60	15.3	Sparsely phyric	JM	0.11	4.89	1.83	0.13	100	354	14.3	3	32	4.5	17.9	3.8	0.8	1.8	0.7	29.8	12	311.5	1			
193-1190B-																									
2R-1, 17	1.67	Sparsely phyric	JM	0.11	4.84	2.20	0.10	100	379	8.9	1.1	19	4.1	15.9	3.6	0.2	1.7	1	32.3	11	272.7	1.4			
2R-1, 39	1.89	Sparsely phyric	JM	0.11	4.84	2.26	0.10	100	380	10	0.9	14	3.5	16.2	3.7	0.1	1.6	1.5	31	11	261.1	1.3			
193-1190C-																									
1R-1, 16	0.16	Sparsely phyric	JM	0.11	4.82	2.22	0.11	100	386	5.9	0.4	14	3.9	16.8	4.1	0.1	4.3	1.2	32.9	11	260	1.4			
2R-1, 10	3.6	Sparsely phyric	JM	0.11	4.76	2.26	0.10	100	370	7.2	1.3	11	4.9	16.3	3.8	0.1	1.9	2.6	32	11	267.7	1.2			
3R-1, 3	13.23	Sparsely phyric	HP	0.11	4.91	2.08	0.10	100	371	27	5	77	4.3	16.8	3.7	2.20	1.47	3	31	11.9	230	2.51			
3R-1, 18	13.38	Sparsely phyric	JM	0.11	5.01	2.31	0.10	100	383	10.8	0.8	11	4.1	16.2	3.8	0.1	1.6	1.3	30.4	11	255.1	1			
193-1189A-																									
1R-1, 12	0.12	Aphyric	HP	0.15	4.55	1.44	0.28	100	271	53	8	92	10.2	18.0	2.6	1.52	1.23	28	24	16.4	338	2.19			
2R-1, 11	9.81	Aphyric	JM	0.12	4.19	2.05	0.21	100	1208	12.6	39.6	610	6.5	17.7	3.2	0.7	2.9	3.4	13.1	13	337	0.9			
193-1189B-																									
11R-3, 3	129.72	Aphyric	HP	0.12	4.52	1.96	0.13	100	510	30	5	167	4.8	18.1	3.2	1.81	1.54	37	24	12.6	264	1.58			

Table T1 (continued).

Core, section, interval (cm)	Depth (mbsf)	Phenocrysts	Analyses	Trace elements (ppm)																		
				U	V	Y	Zr	La	Ce	Pr	Nd	Sm	Eu	Gd	Tb	Dy	Ho	Er	Tm	Yb	Lu	Ti/Zr
193-1188A-																						
2R-1, 10	9.7	Moderately phyric	JM	0.9	16	34.3	119.8	11.9	26.4	3.72	18.7	4.7	1.34	4.66	0.82	5.34	1.23	3.73	0.57	4.11	0.61	26
2R-1, 18	9.78	Moderately phyric	HP	0.81	18	35	106	11.70	24.93	3.63	17.66	4.27	1.21	4.53	0.83	5.62	1.18	3.69	0.57	3.76	0.58	30
2R-1, 20	9.8	Moderately phyric	JM	0.9	21	33.6	124.8	12.2	26.3	3.57	19.3	4.5	1.31	4.65	0.84	5.43	1.24	3.62	0.56	3.85	0.63	25
7R-1, 6	48.26	Moderately phyric	JM	0.9	16	34.7	121.6	12.2	27.6	3.74	19.5	4.4	1.28	4.97	0.81	5.29	1.17	3.58	0.58	3.79	0.62	26
5R-1, 12	33.72	Sparsely phyric	JM	0.8	26	34.9	116	12.1	26.7	3.53	18.7	4.5	1.42	4.69	0.87	5.27	1.19	3.69	0.55	4.15	0.63	32
193-1191A-																						
1R-1, 38	0.38	Aphyric	JM	0.8	18	33.8	112	11.2	25.8	3.48	18	4.5	1.36	4.47	0.81	5.64	1.18	3.7	0.55	3.84	0.61	34
1R-1, 61	0.61	Aphyric	JM	0.8	21	35	114.3	11.6	26	3.49	19	4.6	1.35	4.93	0.87	5.78	1.24	3.64	0.56	4.32	0.65	34
1R-1, 64	0.64	Aphyric	HP	0.71	22	35	115	25.00	26.51	3.77	17.16	4.56	1.25	4.68	0.84	5.79	1.19	3.80	0.55	3.71	0.58	34
1R-1, 75	0.75	Aphyric	HP	0.77	19	31	109	12.57	27.33	3.97	17.83	4.67	1.08	4.88	0.88	5.98	1.27	4.02	0.59	3.93	0.62	35
1R-1, 77	0.77	Sparsely phyric	JM	0.7	24	35.3	116	11.8	26.8	3.55	18.4	4.6	1.5	5.19	0.87	5.63	1.22	3.77	0.58	3.83	0.63	33
2R-1, 12	9.52	Sparsely phyric	JM	0.7	22	34.7	112.9	11.7	25.8	3.46	18.5	4.5	1.38	5.22	0.88	5.72	1.23	3.65	0.58	3.79	0.62	34
2R-1, 76	10.16	Aphyric	JM	0.6	23	39.1	114.4	12	25.8	3.47	17.4	4.7	1.37	4.96	0.88	5.43	1.23	3.63	0.58	3.91	0.61	33
2R-1, 128	10.68	Sparsely phyric	JM	0.7	20	33.1	110	11.8	25.2	3.4	19	4.6	1.3	4.73	0.79	5.34	1.21	3.58	0.53	3.66	0.64	35
2R1, 145	10.83	Sparsely phyric	JM	0.7	25	37.7	122.6	12.4	27.3	3.72	19.8	4.8	1.51	5.33	0.93	6.11	1.24	3.95	0.65	4.33	0.71	31
2R-2, 22	11.12	Sparsely phyric	JM	0.7	23	33.7	109.6	11.4	24.8	3.43	18.8	4.6	1.27	4.71	0.89	5.03	1.14	3.53	0.6	4	0.62	35
2R-2, 88	11.78	Sparsely phyric	JM	0.7	22	35.1	115.8	11.8	27.5	3.56	18.1	4.8	1.41	4.94	0.89	5.72	1.3	3.83	0.56	4	0.59	33
2R-2, 90	11.8	Aphyric	JM	0.7	22	34.8	114.4	11.4	24.1	3.38	17	4.4	1.36	4.85	0.82	5.54	1.19	3.56	0.52	3.75	0.62	34
3R-1, 18	14.88	Sparsely phyric	JM	0.6	24	36.6	117.9	12	26.6	3.71	19.3	4.7	1.45	5.13	0.88	5.61	1.3	3.74	0.64	4.33	0.69	32
3R-1, 60	15.3	Sparsely phyric	JM	0.8	23	36.9	121.7	12.7	27.3	3.83	20.1	4.78	1.47	5.46	0.94	5.78	1.33	3.84	0.58	4.06	0.69	32
193-1190B-																						
2R-1, 17	1.67	Sparsely phyric	JM	0.8	22	34.8	119.3	12.2	26.3	3.6	17.4	4.4	1.24	4.83	0.89	5.62	1.2	3.72	0.59	4.08	0.67	26
2R-1, 39	1.89	Sparsely phyric	JM	0.9	21	33.1	116.9	12.2	26.3	3.54	19.1	4.4	1.27	4.92	0.8	5.19	1.08	3.35	0.59	3.78	0.62	27
193-1190C-																						
1R-1, 16	0.16	Sparsely phyric	JM	1	17	35.1	125.7	12.7	26.4	3.81	19.5	4.3	1.27	4.88	0.9	5.46	1.67	3.74	0.61	3.92	0.63	24
2R-1, 10	3.6	Sparsely phyric	JM	0.8	19	33.6	118	12.4	26.8	3.62	18.8	4.5	1.35	5.11	0.83	5.26	1.23	3.82	0.58	3.89	0.65	27
3R-1, 3	13.23	Sparsely phyric	HP	0.80	17	37	123	11.79	25.68	3.91	17.03	4.29	1.12	4.62	0.80	5.41	1.17	3.72	0.54	3.73	0.58	26
3R-1, 18	13.38	Sparsely phyric	JM	0.8	16	33.9	117.1	12.3	26.2	3.56	18.5	4.4	1.24	4.71	0.83	5.25	1.13	3.54	0.55	3.94	0.6	26
193-1189A-																						
1R-1, 12	0.12	Aphyric	HP	1.26	82	32	93	9.75	23.75	3.38	15.12	4.39	1.39	5.27	0.82	5.23	1.14	3.54	0.50	3.38	0.51	56
2R-1, 11	9.81	Aphyric	JM	0.7	47	31.4	101.3	10.4	23.3	3.4	16.8	4.1	1.41	4.76	0.81	5.18	1.06	3.47	0.52	3.55	0.56	46
193-1189B-																						
11R-3, 3	129.72	Aphyric	HP	0.70	20	34	117	11.02	24.74	3.71	16.37	4.21	1.14	5.01	0.80	5.63	1.18	3.73	0.53	3.54	0.56	33

Table T1 (continued).

Core, section, interval (cm)	Depth (mbsf)	Phenocrysts	Analyses	REE normalized															
				La	Ce	Pr	Nd	Sm	Eu	Gd	Tb	Dy	Ho	Er	Tm	Yb	Lu	La/Yb	Eu/Eu*
193-1188A-																			
2R-1, 10	9.7	Moderately phyric	JM	5.81	1.11	116.79	57.17	614.36	161.90	101.93	64.14	49.08	55.23	6.38	130.90	3.31	140.16	1.756	0.647
2R-1, 18	9.78	Moderately phyric	HP	6.96	1.00	131.46	58.33	543.59	159.18	96.26	62.54	46.35	50.13	5.78	127.26	3.33	147.57	2.088	0.696
2R-1, 20	9.8	Moderately phyric	JM	4.52	1.11	153.28	56.00	640.00	165.99	101.54	61.55	50.66	52.88	6.24	130.62	3.39	142.52	1.333	0.651
7R-1, 6	48.26	Moderately phyric	JM	5.81	1.11	116.79	57.83	623.59	165.99	106.56	64.48	51.18	51.70	6.10	139.61	3.27	138.85	1.778	0.644
5R-1, 12	33.72	Sparsely phyric	JM	2.90	0.99	189.78	58.17	594.87	164.63	103.09	60.86	49.08	52.88	6.76	131.74	3.51	138.32	0.828	0.665
193-1191A-																			
1R-1, 38	0.38	Aphyric	JM	4.19	0.99	131.39	56.33	574.36	152.38	99.61	60.00	47.24	52.88	6.48	125.56	3.27	148.03	1.284	0.637
1R-1, 61	0.61	Aphyric	JM	3.55	0.99	153.28	58.33	586.15	157.82	100.39	60.17	49.87	54.05	6.43	138.48	3.51	151.71	1.011	0.651
1R-1, 64	0.64	Aphyric	HP	7.54	0.88	158.32	58.33	589.74	340.18	102.35	64.94	45.03	53.53	5.95	131.46	3.37	151.98	2.237	1.385
1R-1, 75	0.75	Aphyric	HP	7.03	0.96	137.15	51.67	558.97	171.01	105.51	68.39	46.80	54.93	5.13	136.96	3.56	157.06	1.976	0.704
1R-1, 77	0.77	Sparsely phyric	JM	3.23	0.87	175.18	58.83	594.87	160.54	103.47	61.21	48.29	54.05	7.14	145.79	3.51	147.77	0.920	0.647
2R-1, 12	9.52	Sparsely phyric	JM	2.90	0.87	160.58	57.83	578.97	159.18	99.61	59.66	48.56	52.88	6.57	146.63	3.55	150.13	0.818	0.663
2R-1, 76	10.16	Aphyric	JM	2.58	0.74	167.88	65.17	586.67	163.27	99.61	59.83	45.67	55.23	6.52	139.33	3.55	142.52	0.727	0.675
2R-1, 128	10.68	Sparsely phyric	JM	3.23	0.87	145.99	55.17	564.10	160.54	97.30	58.62	49.87	54.05	6.19	132.87	3.19	140.16	1.013	0.685
2R1, 145	10.83	Sparsely phyric	JM	4.52	0.87	182.48	62.83	628.72	168.71	105.41	64.14	51.97	56.40	7.19	149.72	3.75	160.37	1.204	0.655
2R-2, 22	11.12	Sparsely phyric	JM	4.52	0.87	167.88	56.17	562.05	155.10	95.75	59.14	49.34	54.05	6.05	132.30	3.59	132.02	1.258	0.669
2R-2, 88	11.78	Sparsely phyric	JM	3.55	0.87	160.58	58.50	593.85	160.54	106.18	61.38	47.51	56.40	6.71	138.76	3.59	150.13	0.989	0.639
2R-2, 90	11.8	Aphyric	JM	4.52	0.87	160.58	58.00	586.67	155.10	93.05	58.28	44.62	51.70	6.48	136.24	3.31	145.41	1.366	0.664
3R-1, 18	14.88	Sparsely phyric	JM	5.16	0.74	175.18	61.00	604.62	163.27	102.70	63.97	50.66	55.23	6.90	144.10	3.55	147.24	1.455	0.655
3R-1, 60	15.3	Sparsely phyric	JM	3.23	0.99	167.88	61.50	624.10	172.79	105.41	66.03	52.76	56.17	7.00	153.37	3.79	151.71	0.851	0.674
193-1190B-																			
2R-1, 17	1.67	Sparsely phyric	JM	4.52	0.99	160.58	58.00	611.79	165.99	101.54	62.07	45.67	51.70	5.90	135.67	3.59	147.51	1.258	0.666
2R-1, 39	1.89	Sparsely phyric	JM	4.19	1.11	153.28	55.17	599.49	165.99	101.54	61.03	50.13	51.70	6.05	138.20	3.23	136.22	1.300	0.673
193-1190C-																			
1R-1, 16	0.16	Sparsely phyric	JM	4.52	1.24	124.09	58.50	644.62	172.79	101.93	65.69	51.18	50.53	6.05	137.08	3.63	143.31	1.244	0.674
2R-1, 10	3.6	Sparsely phyric	JM	3.87	0.99	138.69	56.00	605.13	168.71	103.47	62.41	49.34	52.88	6.43	143.54	3.35	138.06	1.157	0.674
3R-1, 3	13.23	Sparsely phyric	HP	8.11	0.99	121.68	61.67	630.77	160.39	99.14	67.49	44.71	50.43	5.34	129.75	3.21	142.10	2.523	0.641
3R-1, 18	13.38	Sparsely phyric	JM	3.23	0.99	116.79	56.50	600.51	167.35	101.16	61.38	48.56	51.70	5.90	132.30	3.35	137.80	0.964	0.679
193-1189A-																			
1R-1, 12	0.12	Aphyric	HP	7.05	1.56	597.37	53.33	476.92	132.65	91.69	58.29	39.69	51.53	6.64	148.12	3.29	137.17	2.141	0.634
2R-1, 11	9.81	Aphyric	JM	2.90	0.87	343.07	52.33	519.49	141.50	89.96	58.62	44.09	48.18	6.71	133.71	3.27	135.96	0.889	0.655
193-1189B-																			
11R-3, 3	129.72	Aphyric	HP	5.09	0.87	147.37	56.67	600.00	149.90	95.53	64.05	42.97	49.51	5.44	140.64	3.22	147.71	1.582	0.626

**Table T2.** Summary of mineral and glass compositions from fresh lavas sampled on Pual Ridge crest.

Average glass composition		Element oxides (wt%)										
CaO value	SiO <sub>2</sub>	TiO <sub>2</sub>	Al <sub>2</sub> O <sub>3</sub>	FeO	MgO	CaO	MnO	Na <sub>2</sub> O	K <sub>2</sub> O	P <sub>2</sub> O <sub>5</sub>	Total	
Site 1188	72.10	0.44	14.02	2.78	0.27	2.08	0.09	4.80	2.20	0.08	98.88	
Site 1189	65.84	0.88	14.91	5.67	0.89	3.84	0.12	4.57	1.68	0.33	98.75	
Site 1190	70.90	0.45	14.14	3.54	0.41	2.18	0.08	4.50	2.33	0.08	98.63	
Site 1191	69.61	0.66	14.25	4.44	0.45	2.75	0.10	4.60	1.95	0.11	98.92	

Plagioclase compositions		Element oxides (wt%)											
CaO value	SiO <sub>2</sub>	Al <sub>2</sub> O <sub>3</sub>	CaO	Na <sub>2</sub> O	K <sub>2</sub> O	Fe <sub>2</sub> O <sub>3</sub>	SrO	Total		Ab	An	Or	
Site 1188	Highest	59.58	24.93	7.23	7.25	0.26	0.38	0.23	99.90		0.35	0.64	0.01
	Lowest	57.24	26.57	9.04	6.07	0.20	0.57	0.16	99.88		0.44	0.54	0.01
Site 1189	Highest (rim)	55.35	27.52	10.02	5.63	0.15	0.76		99.43		0.49	0.50	0.01
	Lowest (core)	56.18	27.59	10.28	5.24	0.14	0.54		99.97		0.52	0.47	0.01
Site 1190	Highest	57.90	25.95	8.65	6.44	0.22	0.49	0.12	99.81		0.43	0.57	0.01
	Lowest	56.32	27.08	9.63	5.85	0.19	0.53	0.15	99.84		0.47	0.52	0.01
Site 1191	Highest	62.81	22.17	6.39	6.09	0.60	1.66	0.10	100.14		0.35	0.61	0.04
	Lowest	55.94	27.40	9.87	5.46	0.13	0.60	0.05	99.49		0.50	0.50	0.01

Average clinopyroxene composition		Element oxides (wt%)										
CaO value	SiO <sub>2</sub>	TiO <sub>2</sub>	Al <sub>2</sub> O <sub>3</sub>	FeO	MgO	CaO	MnO	Na <sub>2</sub> O	K <sub>2</sub> O	Cr <sub>2</sub> O <sub>3</sub>	NiO	Total
Site 1188	51.21	0.37	1.31	11.96	12.97	20.52	0.52	0.31	0.00	0.05	0.00	99.22
Site 1190	51.67	0.32	1.29	12.74	13.23	19.51	0.57	0.31	0.02	0.00	0.00	99.67
Site 1191	51.08	0.47	1.55	12.09	13.94	19.45	0.50	0.31	0.00	0.00	0.00	99.40

Average orthopyroxene composition		Element oxides (wt%)										
CaO value	SiO <sub>2</sub>	TiO <sub>2</sub>	Al <sub>2</sub> O <sub>3</sub>	FeO	MgO	CaO	MnO	Na <sub>2</sub> O	K <sub>2</sub> O	Cr <sub>2</sub> O <sub>3</sub>	NiO	Total
Site 1188	51.31	0.21	0.63	26.78	18.46	1.68	1.08	0.05	0.02	0.01	0.00	100.24
Site 1190	51.59	0.24	0.63	26.02	18.74	1.61	1.10	0.06	0.00	0.00	0.00	99.98
Site 1191	51.87	0.28	1.57	20.49	22.80	1.44	0.68	0.05	0.01	0.06	0.07	99.33

**Table T3.** Summary of lithologic, bulk chemistry, and mineral chemistry data from fresh lavas, Leg 193.

Site	Lithology	Bulk SiO <sub>2</sub> (wt%)	Chemistry Ti/Zr	Mineral textures	Mineral chemistry (plagioclase [An])	Clinopyroxene	Orthopyroxene	Temperature (°C)
1188	Vesicular, plagioclase-pyroxene phyric rhyodacite	69.9	27	Euhedral	37–44	Wo 37.9–42.7	Wo 3.5–3.6	950
1189	Vesicular, aphyric to sparsely plagioclase phyric dacite	67.2	43	Rounded and embayed	49–52			
1190	Vesicular, plagioclase-pyroxene phyric rhyodacite	70.2	26	Rounded	43–47	Wo 40.0–42.7	Wo 3.3–3.5	960
1191	Vesicular, aphyric to sparsely plagioclase-pyroxene phyric rhyodacite	69.6	33	Subrounded to euhedral	37–44	Wo 35.9–42.7 Fs 18.3–21.6	Wo 3.1–4.2 Fs 32.0–35.6	1015

Note: Bulk SiO<sub>2</sub> values are anhydrous. Temperatures calculated from QUILF95 ([www.geosciences.stonybrook.edu/people/faculty/lindsley/lindsley.html](http://www.geosciences.stonybrook.edu/people/faculty/lindsley/lindsley.html)). See also Andersen et al. (1993).